

MASARYKOVA UNIVERZITA
PŘÍRODOVĚDECKÁ FAKULTA
ÚSTAV TEORETICKÉ FYZIKY A ASTROFYZIKY

Bakalářská práce

BRNO 2020

MARTIN CHOBOLA

**Výzkum Slunce s
observatoří ALMA –
seznámení se s
problematikou a řešení
vybraných dílčích otázek**

Bakalářská práce

Martin Chobola

Bibliografický záznam

Autor: Martin Chobola
Přírodovědecká fakulta, Masarykova univerzita
Ústav teoretické fyziky a astrofyziky

Název práce: Výzkum Slunce s observatoří ALMA – seznámení se s problematikou a řešení vybraných dílčích otázek

Studijní program: Fyzika

Studijní obor: Astrofyzika

Vedoucí práce: RNDr. Miroslav Bárta Ph.D.

Akademický rok: 2019/20

Počet stran: 41 + 9

Klíčová slova: Rádiová interferometrie, ALMA, vícekanálová pozorování Slunce

Bibliographic Entry

Author: Martin Chobola
Faculty of Science, Masaryk University
Department of Theoretical physics and Astrophysics

Title of Thesis: Solar research with ALMA – introduction to the topic and solutions for selected particular problems

Degree Programme: Physics

Field of Study: Astrophysics

Supervisor: RNDr. Miroslav Bárta Ph.D.

Academic Year: 2019/20

Number of Pages: 41 + 9

Keywords: Radio interferometry, ALMA, multi-wavelength solar observations

Abstrakt

Mikrovlnná interferometrická observatoř ALMA v Chile, postavená a provozovaná v široké mezinárodní spolupráci ESO, NRAO a NAOJ, je jedinečným zařízením pro astronomický výzkum. Přestože se ALMA věnuje především objektům vzdáleného vesmíru, mezi její vědecké cíle také patří i objekty sluneční soustavy, včetně Slunce. Vzhledem k tomu, že velká většina cílů není solární, observatoř přirozeně používá systém rovníkových souřadnic Ra/Dec (ICRS nebo J2000). Zatímco standard ve sluneční fyzice, užívaný družicovými i pozemními slunečními dalekohledy, je systém tzv. helio-projektivních kartézských (HPC) souřadnic spojených se středem slunečního disku. Praktické získání vědecky využitelných slunečních radiových map z observatoře ALMA, včetně možnosti jejich přímého navázání na obrazová data z jiných observatoří (pozemních i družicových), je tedy poměrně komplikovaný proces (kalibrace a výběr dat, imaging, transformace souřadnic). Práce se soustředí na studium celého tohoto postupu a vyústí ve vlastní příspěvek autora: program, který na základě výše zmíněných znalostí získaných rešerší literatury a praktickým zpracováním cvičných reálných dat z ALMA archívu umožní překládání více-kanálových zobrazení Slunce – ALMA + družicová nebo pozemní optická pozorování – přes sebe.

Abstract

Microwave interferometric observatory ALMA in Chile, built and operated in a wide international collaboration between ESO, NRAO and NAOJ, is one of the kind facility for astronomical research. Although ALMA focuses mainly on objects in outer space, its scientific goals include objects in the solar system, including the Sun, too. Because of vast majority of the targets is non-solar, the observatory naturally uses the system of equatorial Ra / Dec coordinates (ICRS or J2000). On the other hand, standard in solar research, used in satellite and ground-based solar telescopes, is a system of Helio-Projective Cartesian (HPC) coordinates connected to the center of the solar disk. The practical acquisition of scientifically usable solar radio maps from the ALMA observatory, including the possibility of their direct connection to image data from other observatories (terrestrial and/or satellite), is therefore a relatively complicated process (calibration and data selection, imaging, coordinate transformation). The work focuses on the study of the whole process and results in the author's own contribution: a program which, based on the above knowledge of literature search and practical processing of real-world training data from the ALMA archive will enable overlay of multi-channel images of the Sun - over each other.

ZADÁNÍ
BAKALÁŘSKÉ PRÁCE

Akademický rok: 2019/2020

Ústav:	Ústav teoretické fyziky a astrofyziky
Student:	Martin Chobola
Program:	Fyzika
Obor:	Astrofyzika

Ředitel *Ústavu teoretické fyziky a astrofyziky* PŘF MU Vám ve smyslu Studijního a zkušebního řádu MU určuje bakalářskou práci s názvem:

Název práce:	Výzkum Slunce s observatoří ALMA – seznámení se s problematikou a řešení vybraných dílčích otázek
Název práce anglicky:	Solar research with ALMA – introduction to the topic and solutions for selected particular problems
Jazyk závěrečné práce:	angličtina

Oficiální zadání:

Mikrovlnná interferometrická observatoř ALMA, postavená a provozovaná v široké mezinárodní spolupráci ESO, NRAO a NAOJ, je jedinečným a špičkovým zařízením pro astronomický výzkum. Od svého vzniku má na kontě mnoho průlomových objevů a byla i naprosto klíčovým elementem globálního VLBI interferometru EHT, který nám v dubnu 2019 přinesl vůbec první snímek blízkého okolí černé díry v galaxii M87.

Přestože se ALMA věnuje především objektům vzdáleného vesmíru, mezi její vědecké cíle patří i objekty sluneční soustavy, včetně Slunce. Vědecký výzkum Slunce s obs. ALMA má – oproti studiu vzdálených objektů – ovšem i svoje zvláštnosti: mimo jiné, kvůli vysokému jasů na mm vlnách a relativnímu pohybu objektů na Slunci (např. skvrn) vůči vzdáleným hvězdám (v důsledku denního pohybu a diferenciální rotace Slunce, což lze popsat vhodnou efemeridou) potřebuje specifickou kalibrační proceduru. Protože emise vždy zabírá celé zorné pole antény, je nutné obrazy získané interferometricky (INT) kombinovat s daty získanými skenováním pomocí jedné antény (tzv. TP data). A protože ALMA je primárně určena pro vzdálený vesmír, pracuje přirozeně v systému rovníkových Ra/Dec souřadnic (ICRS nebo J2000), zatímco standard ve sluneční fyzice, užívaný družicovými i pozemními optickými slunečními dalekohledy, je systém tzv. helio-projektivních kartézských (HPC) souřadnic spojených se středem slunečního disku. Praktické získání vědecky využitelných slunečních radiových map z observatoře ALMA, včetně možnosti jejich přímého navázání na obrazová data z jiných observatoří (pozemních i družicových), je tedy poměrně komplikovaný proces zahrnující (1) specifickou kalibraci a výběr primárních dat, (2) interferometrické zobrazení (imaging) kalibrované datové sady, (3) kombinaci INT obrazů s TP pozorováním, a (4) transformaci získaného výsledného FITS obrazu do systému slunečních HPC souřadnic.

Práce se soustředí na studium celého tohoto postupu a vyústí ve vlastní příspěvek autora k některým jeho krokům. Jejím cílem je důkladné seznámení se s metodou radiové interferometrie, jejími matematickými základy, principy kalibrace dat a získání interferometrického obrazu. Použití metody bude demonstrováno na reálných pozorovacích datech z archivu observatoře ALMA. Konkrétní aplikace se soustředí na sluneční pozorování a jejich specifika – kalibrace, kombinace INT+TP dat, efemerida a transformace souřadnic. Praktickým výstupem práce bude program, který na základě výše zmíněných znalostí získaných rešerší literatury a praktickým zpracováním cvičných reálných dat umožní překládání více-kanálových zobrazení Slunce – ALMA + družicová nebo pozemní optická pozorování – přes sebe. Program zcela jistě najde uplatnění ve vědecké komunitě při multi-frekvenční analýze slunečních pozorování.

- Thompson, A.R., Moran, J.M., Swenson Jr, G.W. (2001).: Interferometry and Synthesis in Radio Astronomy, Wiley ISBN: 978-0471254928
- Budějický, J., Plavcová, Z., Plavec, M. (1962): Radioastronomie, NČSAV Praha
- Wilson, T.L., Rohlfs, K., Hüttemeister, S. (2009): Tools of Radio Astronomy, Springer, ISBN: 978-3- 540-85121-9
- Marr, J.M., Snell, R.L., Kurtz, S.E (2015): Fundamentals of Radio Astronomy: Observational Methods, CRC Press, ISBN:978-1420076769

Vedoucí práce: RNDr. Miroslav Bárta, Ph.D.

Datum zadání práce: 20. 11. 2019

V Brně dne: 13. 5. 2020

Poděkování

Zde bych chtěl poděkovat především mému vedoucímu doktoru Miroslavu Bártovi za jeho ochotu a toleranci při konzultacích a nesmírnou pomoc při psaní práce. Také bych chtěl poděkovat všem, kteří mi pomohli se dostat až sem.

Prohlášení

Prohlašuji, že jsem svoji bakalářskou práci vypracoval samostatně s využitím informačních zdrojů, které jsou v práci citovány.

Brno 31. května 2020

.....
Martin Chobola

Contents

Introduction	1
1. Radio interferometry	5
1.1 Mathematical foundations of aperture synthesis	6
1.2 Problems with real data - basics of calibration of interferometric measurement	13
1.3 Modern interferometric observatories	16
2. Solar research with the ALMA	21
2.1 What can ALMA tell us about the Sun	21
2.2 How can we make ALMA observing the Sun	22
3. Procedure for the transformation of solar data from the ALMA observatory: own contribution to the scientific use of solar observations	25
4. Conclusion	33
References	35
Appendix	36

Introduction

Since 2016 astrophysics knows three ways of studying objects in our Universe: Via material information carriers such as meteorites, cosmic ray particles or the samples collected by the space probes in our closest cosmic vicinity, by means of analysis of electromagnetic radiation of all kinds and, most recently, also by studying the signals of gravitational waves. From all of them, however, the electromagnetic radiation remains the far dominant source of our information about remote cosmic bodies and this status likely will not change soon.

From the beginning of time, our studies of the Universe mediated through the electromagnetic radiation, were carried out only in the wavelengths visible by human eye, until William Herschel in 1800 discovered near infrared and Johann W. Ritter in 1801 ultraviolet radiation (see [Wilson et al. \(2009\)](#)). Nevertheless, with the terrestrial atmosphere blocking those kinds of radiation and no available technology for their quantitative detection, no progress in opening a new spectral window for the astrophysical exploration had been done, until 1931. In that year, Karl Guthe Jansky, searching for the source of noise in the wireless communication devices, discovered that part of the unwanted signal actually comes from the deep space. Thus, it was found that the radio waves – known already since times of Maxwell and Hertz to be, akin of the light, the part of the electromagnetic spectrum – can be generated (besides the man-made devices) also by the matter in space. The Jansky’s paper (see [Jansky \(1933\)](#)) on that topic is considered as a birth of a new research discipline in astrophysics – the radio astronomy. Many other pioneers ([Reber \(1940\)](#), [Hey \(1946\)](#)) continued in his work; they improved measurements by bigger telescopes and better receivers and identified many discrete radio sources on the sky, among them also our Sun. And after the World War II the radio astronomy has been already established as a ‘classical’ part of our astrophysical research.

Thanks to technological advances after 1960’s, namely the breakthrough in our research carried out from the space, new observing windows have been opened in the entire spectrum of the electromagnetic waves. High-flying aircrafts, balloons, and satellites like ISO, IRAS and MSX allow observations in the mid and far infrared; satellites like IUE for ultraviolet and CHANDRA for X-rays; and many others allow measurements from γ - rays to wavelengths longer than 10^4 m. Nevertheless, in spite of steeply growing number of space-research facilities, the ground-based radioastronomy, which has for the first time broken the visible-light limits for our exploration of the Universe, does not by any means loose its potential. The opposite is true – recent technological revolution in the digital signal processing has brought stormy development to the radio astronomy, too. Namely, it is interferometry and aperture synthesis with large antenna arrays connected to powerful dedicated supercomputers — correlators, what experiences unprecedented expansion in modern times. For every telescope, bigger means better, especially in radioastronomy.

With usually weak radio brightness of cosmic bodies and limits, of how large we can build telescopes, we need more efficient way to collect, already so scarce, radiation, and that is interferometry. The method is rooted in forming large antenna arrays, which – when properly interconnected – act like a single large telescope. The strong development of this method is recently witnessed by construction of new and better radio observatories such as ALMA (see Fig.2) , LOFAR, GMRT, MWA, Noema, and further, yet larger instruments are going to be built (e.g., SKA, upgrade of LOFAR to LOFAR-2, etc.).

Larger arrays not only have bigger collecting area but also their increased linear dimensions improve spatial resolution, with which we are able to observe our science targets. This is another important quality of observation, in addition to the already touched sensitivity, which gets improved by increasing total antenna area and also thanks to the modern more sensitive low-noise amplifiers and detectors. At the same moment, technological advance helped us to shift the interferometric radio observations towards the very short – mm and sub-mm – wavelengths (or, in terms of frequencies, into the THz range). This spectral range in between infrared and 'classical' radio wavelengths has been, until recently, a *terra incognita*, with just a few single-dish instruments working at the sub-THz and THz frequencies. Coming age of mm arrays like SMA, ATCA, Carma, Noema-2/IRAM-PdB, and above all the far largest in this category – ALMA, has changed the situation rapidly and brought a real revolution into our astrophysical research. Namely, combination of the short observed wavelengths and long baselines (i.e., the linear dimensions of the antenna array) leads to ,until now, far unreachable spatial resolution of mm interferometric systems. After success of the long-baseline ALMA campaign ([ALMA Partnership 2015](#)) and first trans-atlantic mm-VLBI connection (ALMA–IRAM, 2015) the dream of the Event Horizon Telescope (EHT) has come true (see Fig.1) and resulted in the famous first picture of the vicinity of the black hole in the center of M87 galaxy, published in April 2019. Let us note, that ALMA played a key role in the global mm-VLBI array of the EHT – its far larger total antenna collecting area increased sensitivity of the entire EHT system by factor of ten. And since that big success, the global mm VLBI network centered around ALMA has started to be used more routinely – mm VLBI projects can be now requested during standard ALMA call for observing-time proposals.

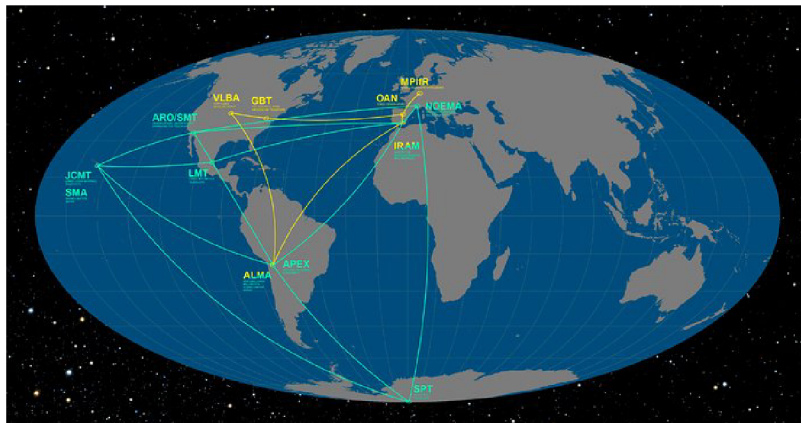


Figure 1: The Event Horizon Telescope and Global mm-VLBI Array on the Earth ([ESO/C., Furtak 2017](#)).

Not only in this respect, observatory ALMA is the global leading player in mm interferometry for this and likely also for a couple of future decades. With its 66 parabolic dishes – 54 twelve-meter and 12 seven-meter, spread over 15 km of dry Atacama dessert in Chile, ALMA is multinational project built and operated namely by joint efforts of European South observatory (ESO), American National Radio Astronomy Observatory (NRAO) and National Astronomical Observatories of Japan (NAOJ). ALMA has been officially commissioned as 'finished/ready for science' in March 2013, nevertheless its further development since that time still continues: For example, a new correlator, extension of baselines up to 32 km, new ultra low-noise multi-feed detectors, or opening so-far unimplemented observing-frequency bands, are planned for the next decade. One class of the important improvements of ALMA capabilities is rooted in development of new observing modes. The specific *Solar ALMA Observing Mode*, which has been in its basic version commissioned (also thanks to the contribution of the [ALMA Czech node \(2017\)](#) of EU ARC) in early 2017 and allowed for solar observations with ALMA, can serve as one of the examples. Although ALMA observing projects mostly focus on galaxies, interstellar matter, and further objects in the deep Universe, The "Stellar evolution and the Sun" represents one of the five major ALMA research topics. And indeed, ALMA can help us a lot with understanding many so far open key questions in solar physics, too, for example, heating of the upper chromosphere and corona, coronal magnetism etc. ([Bastian et al. 2018](#)).



Figure 2: The Atacama Large Millimeter/submillimeter Array (ALMA) by night, under the Magellanic Clouds ([ESO/C., Malin 2012](#)).

Solar ALMA ObsMode is – since 2017 – used for standard solar research. Nevertheless, procedures for observing and especially processing the images of the Sun acquired by ALMA are still under development. One of the procedures, which is still completely missing and will help a lot to scientific exploitation of the solar ALMA observations, is a co-alignment of the calibrated synthesised images of the Sun from ALMA with similar data obtained by the other modern instruments, namely the space-born telescopes, e.g. on-board missions like Hinode, IRIS or SDO. While ALMA works in the standard geocentric equatorial coordinates of ICRS system (α, δ), in which the Sun slowly moves during the

observation (because of yearly motion and also due to the differential rotation of the Sun), the modern solar image data are almost solely in the reference frame fixed to the solar-disk center, in the so called Helio-Projective Cartesian coordinates – HPC (x, y) . To that end, a procedure, which – using the ephemeris connected with the observed target at the Sun – will transform the solar ALMA images into the (in solar-physics *de facto* standard) HPC, is required. Development and testing of software that would perform this necessary transformations and would eventually become a part of Solar ALMA SW package is – aside of getting deep expertise in the (solar) mm interferometry – one of the main tasks of this thesis.

1. Radio interferometry

Even though first observation of extraterrestrial radio waves had been made in 1930s by Jansky and Reber, major advances in what later came to be called *radio astronomy* took after the World War II. Not merely radiometry, i.e. measuring of light-curves of the astrophysical radio sources, but also other disciplines (in analogy with existing methods in optical astronomy) have developed: (radio) spectroscopy, polarimetry, and of course, imaging, i.e., creating the radio maps – monochromatic and later multi-frequency images of the radio sources. The last one is demanding in the radio domain if we take into account that angular resolution of the telescope is $\approx \lambda/D$, where λ is a (relatively long) wavelength and D the size of the instrument. Since single dishes cannot increase their diameters above some technical limits (currently, the largest single-dish instrument is the Chinese immovable telescope FAST with illuminated diameter $D \approx 300\text{ m}$), the way out lays in forming large, mutually connected antenna systems, where the size D can reach much larger value (currently, in practice, the Earth diameter, but even larger system including stations in space are tested and planned). This method is called *radio interferometry* and it has become the most powerful tool of modern radio astronomy.

Beginnings of radio interferometry can be traced to England right after the WWII, where J.A. Ratcliffe, Martin Ryle and Derek Vonberg made the first two-element radio interferometer (Ryle & Vonberg 1946). Later, Graham Smith joined Ryle’s group and implemented a phase-switcher for combining two signals (Ryle et al. 1950). In mid-50s, development of multiantenna arrays for centimetre-wavelength solar measurements has started.

Early interferometers have been working on *additive* principle, similarly to the double-slit experiment by Young, or as it is used in optical gratings for (optical) spectroscopy. This is easy to implement, since the signal from the antennas can be summed by analog electrical circuits. In early 60s, a different principle based on *correlations*, i.e., multiplication of digitised signals from two antennas, started to be utilised. Albeit this principle has been known since 1930’s (as we describe right in the following), its application had to wait for advancement in digital and computing technology. The digital, correlation-based interferometry – also known as *aperture synthesis* – has many advantages to the older analog additive systems (phased arrays). Among them namely: (1) It is much easier to obtain multi-frequency radio images (i.e., 3D data cubes) of the radio sources and, (2) Correlations of the digitized signals can be computed *ex post* if the both signals contain synchronised time stamps. Hence, the remote antennas need not to be even physically connected, provided that the synchronisation is reached different way (typically via atomic clock). This enables systems with very long distances between antennas (i.e. baselines) – Very Long Baseline Interferometry/VLBI.

Because of increasing significance of aperture synthesis in the radioastronomical research, as well as in order to approach the core of this work, in the following we shall

tackle solely this modern method based on the (digitised) signal correlations.

1.1 Mathematical foundations of aperture synthesis

The signal-correlation interferometry is based on *van Zitter-Cernike theorem* (van Cittert (1934) and Zernike (1938)), which effectively claims that correlation of signals from two antennas corresponds to a single Fourier component of the 2D radio brightness distribution on the sky (radio map, radio image). Which Fourier component it is, it depends on geometry – position vectors of the two antennas and the direction towards the source – and the wavelength used for observation. In the following a loose “proof” of the theorem will be presented, the exact analysis and details can be found in Born & Wolf (1965).

Let us start with definition of the correlation function between two signals (voltages), here measured at antennas at the positions \mathbf{r}_1 and \mathbf{r}_2 . Should the signal at the *Antenna 2* be delayed by (so far general) time interval τ , the correlation function $\Gamma_{12}(\mathbf{r}_1, \mathbf{r}_2, \tau)$ reads:

$$\Gamma_{12}(\mathbf{r}_1, \mathbf{r}_2, \tau) = \langle U_1(\mathbf{r}_1, t)U_2^*(\mathbf{r}_2, t - \tau) \rangle = \lim_{T \rightarrow \infty} \frac{1}{2T} \int_{-T}^T U_1(\mathbf{r}_1, t)U_2^*(\mathbf{r}_2, t - \tau) dt \quad (1.1)$$

Here U_1 and U_2 are voltages measured by antennas 1 and 2, respectively, the asterisk ‘*’ denotes complex conjugation, and ‘ $\langle \dots \rangle$ ’ represents time average.

For the sake of simplicity, let us suppose for the beginning, that signal U_i at the antenna i is due to the monochromatic wave with frequency ν ($\omega = 2\pi\nu$, $\lambda = c/\nu$) and a complex amplitude \hat{E}_0 , originating in a single-point source which – because of the very large distance of the source – is a plane wave:

$$U_i(\mathbf{r}_i, t) = \hat{G}_i(\mathbf{k})\hat{E}_0 e^{i(\mathbf{k} \cdot \mathbf{r}_i - \omega t)} \quad (1.2)$$

Here $\hat{G}_i(\mathbf{k})$ is a complex *gain* of the antenna i for the waves with the wavevector \mathbf{k} , whose size is $k = \frac{2\pi}{\lambda}$ and direction just opposite to the unit direction vector \mathbf{s} , pointing towards the (element of) the radio source, i.e., $\mathbf{k} = -k\mathbf{s}$ (see Fig 1.1). The gain expresses namely directivity of the antenna, but includes also description of the antenna and receiver imperfection. If the antennas are pointed to our single-point source and their gain normalized to unity ($G_i^{max} = 1$), the correlation function would be:

$$\Gamma_{12}(\mathbf{r}_1, \mathbf{r}_2, \tau) = |E_0|^2 e^{i[\mathbf{k} \cdot (\mathbf{r}_1 - \mathbf{r}_2) - \omega\tau]} \quad (1.3)$$

In reality, the radio source is rarely an (unresolvable) single-point source and has its structure. To mimic it, we can imagine that the wavefield at the antenna i is a sum of contributions from all N point-like elements of the source:

$$E_i(\mathbf{r}_i, t) = \sum_n^N E_n(\mathbf{r}_i, t), \quad (1.4)$$

where the contributions from the n -th point of the structured source are

$$E_n(\mathbf{r}_i, t) = \hat{E}_n e^{i(\mathbf{k}_n \cdot \mathbf{r}_i - \omega t)} \quad (1.5)$$

Here, the notation E_n is just a shortcut for electric amplitude of the wave propagating from the direction determined by the wave vector \mathbf{k}_n , i.e., $\hat{E}_n \equiv \hat{E}(\mathbf{k}_n)$.

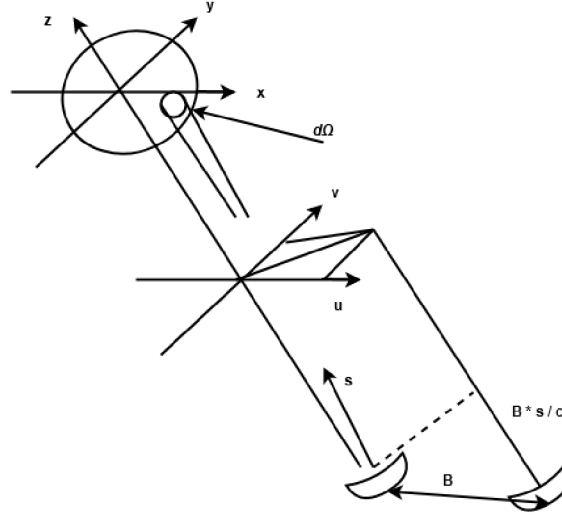


Figure 1.1: To the van Zittert-Cernike theorem: Geometry of the two-element interferometer and the radio source (by author).

Now, let us suppose that the radiation coming from two distinct points m and n in the radio source is mutually incoherent, i.e. relative phases of the two waves are random. In such a case

$$\langle E_m(\mathbf{r}_1, t) E_n^*(\mathbf{r}_2, t - \tau) \rangle = 0 \quad \text{for all } m \neq n \quad (1.6)$$

while

$$\langle E_n(\mathbf{r}_1, t) E_n^*(\mathbf{r}_2, t - \tau) \rangle = |\hat{E}_n|^2 e^{i[\mathbf{k} \cdot (\mathbf{r}_1 - \mathbf{r}_2) - \omega\tau]} \quad (1.7)$$

Let us substitute Eqs. 1.4 and 1.5 into the relation for antenna voltages (Eq. 1.2, just generalized for a sum of the plane waves), and subsequently into the definition of the correlation function:

$$\Gamma(\mathbf{r}_1, \mathbf{r}_2, \tau) = \left\langle \sum_n^N \sum_m^N \hat{G}_1(\mathbf{k}_m) \hat{E}_m e^{i[\mathbf{k}_m \cdot \mathbf{r}_1 - \omega t]} \hat{G}_2^*(\mathbf{k}_n) \hat{E}_n^* e^{-i[\mathbf{k}_n \cdot \mathbf{r}_2 + \omega(t - \tau)]} \right\rangle \quad (1.8)$$

If we now make use of the random-phase (incoherent source) assumption expressed by Eqs. 1.6 and 1.7, only summing over the “diagonal” in the double sum in Eq. 1.8 remains, and the expression for correlation simplifies to

$$\Gamma(\mathbf{r}_1, \mathbf{r}_2, \tau) = \sum_n^N \hat{G}_1(\mathbf{k}_n) \hat{G}_2^*(\mathbf{k}_n) \hat{E}_n \hat{E}_n^* e^{i[\mathbf{k}_n \cdot (\mathbf{r}_1 - \mathbf{r}_2) - \omega\tau]} \quad (1.9)$$

Let us now come from the view of the source as an ensemble of N point sources to the more natural continuous brightness distribution. The summing is thus transformed into integral. Since expression in Eq. 1.9 for the correlation between two antennas 1 and 2 depends just on the vector $\mathbf{B}_{12} \equiv \mathbf{r}_2 - \mathbf{r}_1$ that connects those antennas, and which we call a *baseline*, the *baseline correlation function* can be (in the continuous notation) expressed as

$$R(\mathbf{B}_{12}, \tau) \equiv \Gamma_{1,2}(\mathbf{r}_1, \mathbf{r}_2, \tau) = \int_{\Omega} \hat{G}_1(\mathbf{k}) \hat{G}_2^*(\mathbf{k}) |\hat{E}(\mathbf{k})|^2 e^{i[\mathbf{k} \cdot \mathbf{B}_{12} - \omega\tau]} \Omega \quad (1.10)$$

where integration runs over the (angular) area of the source. If we come from the wave vector \mathbf{k} to more practical quantities characterising the radiation, like the direction vector \mathbf{s} and frequency ν (using the simple relations adduced above), we eventually arrive to the following expression for the baseline correlation function:

$$R(\mathbf{B}_{12}, \tau) = \iint_S A(s) I(s) \exp[i2\pi\nu(\frac{\mathbf{B}_{12} \cdot \mathbf{s}}{c} - \tau_i)] s \nu, \quad (1.11)$$

where $I(\mathbf{s}) = |\hat{E}(\mathbf{s})|^2$ is intensity of radio radiation coming from the direction \mathbf{s} (in proper units), and $A(\mathbf{s}) \equiv G(\mathbf{s})G^*(\mathbf{s})$ is the antenna effective area. The delay τ_i is (so far arbitrary) *instrumental delay* inserted into the signal path of one of the antennas of the two-element interferometer. The (outer) integral over ν also indicates that in reality the output voltage correlations always result from finite (albeit usually very small) frequency bandwidth selected by a filter from the actual non-monochromatic radiation emitted by the source. For a narrow-band frequency channels we can stay with a quasi-monochromatic approximation and replace the integration by merely multiplying by the bandwidth $\Delta\nu$.

Let us now assume that the source does not have very large angular extent on the sky (for large sources we have to repoint usually well directive parabolic antennas anyway, this technique is called *interferometric mosaicing*). In such a case we can split the direction vector \mathbf{s} , pointing to the source element into *reference direction* \mathbf{s}_0 and a small offset $\boldsymbol{\sigma}$

$$\mathbf{s} = \mathbf{s}_0 + \boldsymbol{\sigma} \quad (1.12)$$

Now, the Eq.1.11 can be written as

$$R(\mathbf{B}, \tau_i) = \exp[i\omega(\frac{\mathbf{B} \cdot \mathbf{s}_0}{c} - \tau_i)] \Delta\nu \int_S A(\boldsymbol{\sigma}) I(\boldsymbol{\sigma}) \exp\left(\frac{i\omega\mathbf{B} \cdot \boldsymbol{\sigma}}{c}\right) \boldsymbol{\sigma} \quad (1.13)$$

The result is generally valid for any baseline \mathbf{B} , so we skip the indices 1, 2.

The total signal delay at the second antenna τ can be written as

$$\tau = \tau_g - \tau_i = \frac{\mathbf{B} \cdot \mathbf{s}_0}{c} - \tau_i \quad (1.14)$$

where τ_g represents the delay between two signals coming from the reference direction \mathbf{s}_0 caused by the geometry of the source and the two antennas. In order to correlate a given received photon with “itself”, we tend to the total delay τ to be zero. In addition to reach the time coherence of the signal, there is yet another reason why the instrumental delay τ_i is going to be chosen at such amount that it fully compensates the geometrical delay τ_g , so that total delay $\tau = 0$. The deeper analysis (omitted here for simplicity) that takes into account finite (frequency) bandwidth of the received waves (i.e., that the source is not monochromatic and/or our filter is not described by a delta function) shows that we would have significant decoherence if the total delay is not suppressed by a proper choice of the instrumental displacement of the signal τ_i . Having the τ_i set properly, the baseline correlation function $R(\mathbf{B})$ can be rewritten as

$$V(\mathbf{B})\Delta\nu \equiv R(\mathbf{B}, \tau_i = \tau_g) = \int_S A(\boldsymbol{\sigma}) I(\boldsymbol{\sigma}) \exp(i\frac{\omega\mathbf{B} \cdot \boldsymbol{\sigma}}{c}) \boldsymbol{\sigma} \quad (1.15)$$

This is the *visibility function* (or, just shortly *visibility*, also *interferometric visibility*) for the baseline \mathbf{B} connecting two antennas.

Now, let us write the vector relations in the coordinate system according to Fig. 1.1:

$$\frac{\omega}{2\pi c}\mathbf{B} \equiv (u, v, w) \quad (1.16)$$

where u, v, w are measured in wavelengths, the direction $(0,0,1)$ is parallel to \mathbf{s}_0 , u points to local east direction and v points to north; the vector $\sigma = (x, y, z)$ is defined such that x and y are the direction cosines with respect to the u and v axes, then the xy plane is a projection of the celestial sphere onto a tangent plane with the origin point at \mathbf{s}_0 . In those coordinates (Eq. 1.15) becomes

$$V(u, v, w) = \int_{-\infty}^{\infty} \int_{-\infty}^{\infty} A(x, y)I(x, y) \times \exp[i2\pi(ux + vy + w\sqrt{1-x^2-y^2})] \frac{dxdy}{\sqrt{1-x^2-y^2}} \quad (1.17)$$

As the radiation pattern of the antenna is basically zero outside of its primary beam, we could extend the integration limits (over the source size) to $\pm\infty$.

For the small source (and/or small primary beam - see the note above about mosaicing) we can approximately write $\sqrt{1-x^2-y^2} \approx 1$ and Eq. 1.17 becomes

$$V(u, v, w)e^{i2\pi w} = \int_{-\infty}^{\infty} \int_{-\infty}^{\infty} A(x, y)I(x, y)e^{i2\pi(ux+vy)} dxdy. \quad (1.18)$$

For the same reason, the third component w , which applies only as a correction between the plane image of the source and real spherical section on the sky, is zero for a small source, we can write

$$V(u, v, w)e^{i2\pi(ux+vy)} \approx V(u, v, 0). \quad (1.19)$$

Hence, we arrive to the final relation

$$V(u, v, w=0) = \int_{-\infty}^{\infty} \int_{-\infty}^{\infty} A(x, y)I(x, y)e^{i2\pi(ux+vy)} dxdy. \quad (1.20)$$

This is the van Zittert-Cernike theorem in formulation suitable for radio and mm interferometry based on the measuring of 2-antenna correlations.

The application is – in theory – straightforward: If we do inverse Fourier transform (IFT) of Eq. 1.20, we get

$$I'(x, y) = A(x, y)I(x, y) = \int_{-\infty}^{\infty} V(u, v, 0)e^{i2\pi(ux+vy)} dudv, \quad (1.21)$$

where $I'(x, y)$ is the intensity $I(x, y)$ modified by the primary beam shape $A(x, y)$. Hence, in principle, we (i) measure the signals, digitize it and calculate the visibilities $V(u, v)$ for all pairs of antennas in the array, (ii) Make the IFT according to Eq. 1.21, and (iii), Divide the obtained real image $I'(x, y)$ by the antenna pattern $A(x, y)$ – making so called *primary-beam correction*. This way we get the radio map — real image of the source. This method is called *aperture synthesis*.

In practice, there are several technical issues that we tackle in detail later: (1) The visibilities $V(u, v)$ are biased by many non-ideal effects caused by the instrument or the Earth's atmosphere – this can be to some extent fixed by procedure known as *calibration*, described below, and (2) we work with only limited number M of antennas in the array,

which gives us $\frac{M(M-1)}{2}$ pairs and every pair is a Fourier components for one wavelength and for one time instant. So that is only a sample of all the visibilities, which are noisy samples of a smooth function. Unfortunately, this may and will contain artefacts. In ideal situation, we would measure amplitude and phase for a full uv plane and could determine the intensity distribution $I'(x, y)$ by applying the Fourier transformation (Eq. 1.21). But due to $V(u, v)$ being sampled only at discrete points within a radius $\cong u_{max}$ along elliptical tracks, and in some regions of (u, v) plane, not being measured given by missing shorts spacing, antenna shadowing or a missing angular wedge in the orientation of the baseline vector \mathbf{B} . For a discrete number of visibilities, we have a version of Eq. 1.21, but using summation instead of integral, to get an image by a discrete Fourier transform (DFT):

$$I_D(x, y) = \sum_k A(u_k, v_k) V(u_k, v_k) e^{-i2\pi(u_k x + v_k y)}. \quad (1.22)$$

Sadly, the reconstructed image I_D is not a good representation of the intensity distribution I' , but they are related. We can write Eq. 1.22:

$$I_D(x, y) = P_D(x, y) \otimes I'(x, y), \quad (1.23)$$

where P_D is response to a point source (also called a *dirty beam*) and equals to

$$P_D = \sum_k A(u_k, v_k) e^{-i2\pi(u_k x + v_k y)} \quad (1.24)$$

This is the *point spread function* PSF for the dirty beam. Therefore the dirty beam can represent a transfer function that distorts the image, which is produced by the Fourier transform of the point source in the sampled regions. Both sums in Eq. 1.22 and Eq. 1.24 are calculated over the same positions (u_k, v_k) , which means both side lobe structures of the beam depends on the distribution of these points. The *dirty map* is only a representation of the principal solution and has many negative intensity artefacts, but they are not real and should be removed. The *dirty map* is rather unstable, it can drastically change when more visibility data are added. Instead of a principle solution that assumes $I = 0$ for all unmeasured visibilities, values for V should be adopted at positions in the (u, v) plane, which can be obtained from some plausible method for intensity distribution. This method can be the CLEANing method, which approximates the actual but unknown intensity distribution $I(x, y)$ by superposition of the finite number of point sources with positive intensity A_i placed at positions (x_i, y_i) . The main goal of CLEAN is to figure out the $A_i(x_i, y_i)$ such that

$$I''(x, y) = \sum_i A_i P_D(x - x_i, y - y_i) + I_\epsilon(x, y) \quad (1.25)$$

where I'' is the dirty map obtained from the inversion of the visibility function, P_D is the dirty beam and $I_\epsilon(x, y)$ is the residual brightness distribution after decomposition. Approximation of Eq. 1.25 is depending on order of the noise of I_ϵ . This can not be done analytically, but rather iteratively. The following text and Figs 1.2— 1.5 loosely follows presentation by Wilner (2010).

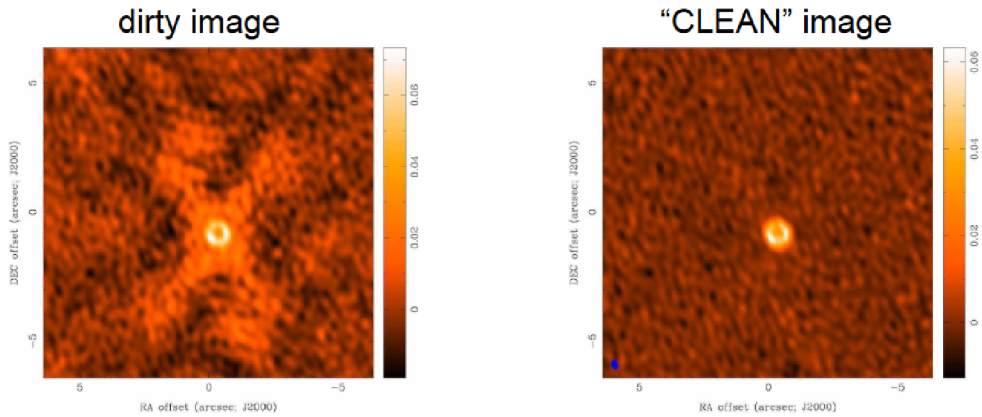


Figure 1.2: CLEAN method.

Högbom (1974) was the first to devise the concept of CLEAN. As said, it is an iterative method which finds the peak intensity of the dirty image and subtracts a fraction γ with the shape of the dirty beam from the image. This will be repeated n times. This *loop gain* $0 < \gamma < 1$ helps the iteration converge, and it continues till the intensity of remaining peaks are below some set limit. Then it is usually the resulting point source model convolved with a *clean beam*, typically of Gaussian shape with FWHM similar to the dirty beam. If this method produces a realistic image, is still unanswered, but Schwarz (1978) has been able, under some conditions, prove its validity. It exist many modifications of the CLEAN method, that can reduce the computing time and/or be customized for specific data.

The Clark CLEAN algorithm (Clark 1980) tries to reduce computing time for large images. It searches only the largest residuals, working with only a sub-region of the beam for much of the time. For smaller images or small beam patches, Högbom CLEAN may still be faster.

The Maximum Entropy Deconvolution Method (MEM) is often used to produce a single optimal image from a set of separate but contiguous images. It solves the problem of selecting the "best" image from many possible images which all agree with the measured visibilities. This method is better suited for multi-field images due to better handling of sources larger than telescopes primary beam.

Moreover, the samples — visibilities are not on the Cartesian grid which troubles the IFT calculations. With even modest data set, computation is time consuming, therefore for inverting Eq.1.20 it is used fast Fourier transform (FFT). But for us to be able to use this method, the visibility function must be placed of regular grid with total sizes that are power of two of the sampling interval. Observed data is seldom on such grid, so we need to use a convolution procedure. The *gridded visibility function* may be represented by

$$I''(u, v) = III(u, v)G(u, v) \otimes I'(u, v), \quad (1.26)$$

where $I'(u, v)$ is the measured function sampled on the irregular u_i, v_i grid, $G(u, v)$ is a convolving function, \otimes is the convolution operator by which a value for an interpolated function $I''(u, v)$ is defined for every u, v and

$$III(u, v) = \Delta u \Delta v \sum_{j, k=-\infty}^{\infty} \delta(u - j \Delta u) \delta(v - k \Delta v) \quad (1.27)$$

which defines the regular grid on the uv plane with Δu and Δv being the pixel size. Now, we get the intensity distribution $I'(x, y)$ by substituting Eq.1.27 into Eq.1.21 and it can be finally computed.

$$I(x, y) = III(u, v) \otimes [G(u, v)I'(u, v)] \quad (1.28)$$

By using Fourier transform on gridded uv data we get an image with a resolution corresponding to the size of the array.

There is also one free parameter and that is weight $W(u, v)$. Till now it was $W(u, v) = 1$, but it can be changed for specific needs. Two most common are natural and uniform. Natural is

$$W(u, v) = \begin{cases} \frac{1}{\sigma^2(u, v)} & \text{for } V(u, v) \neq 0 \\ 0 & \text{for } V(u, v) = 0. \end{cases}$$

This gives more weight to short baselines, which maximizes the point source sensitivity but degrades resolution; is useful for large spatial scales.

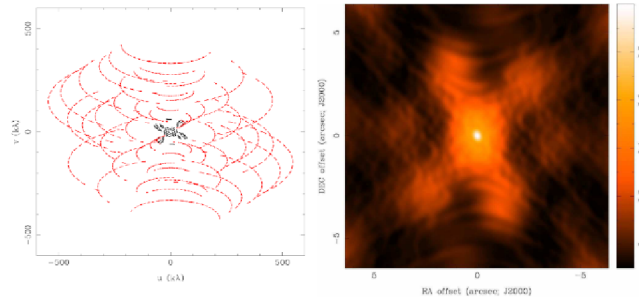


Figure 1.3: Natural weighting.

Uniform weighting is the opposite and it consist in selecting the weights $W(u, v)$ so that the sum of weights $\sum W(u, v) \times A(u, v)$ over a uv cell is a constant function (or zero if no uv data exist in that cell). It gives more weight to long baselines, therefore have higher angular resolution but has lower point source sensitivity.

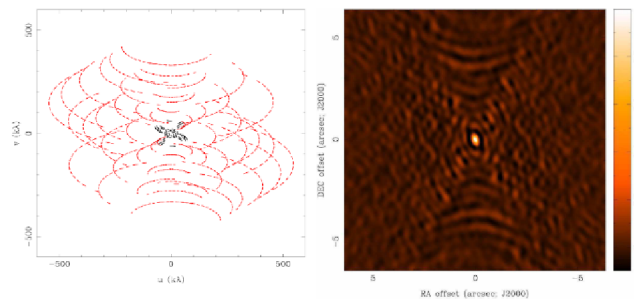


Figure 1.4: Uniform weighting.

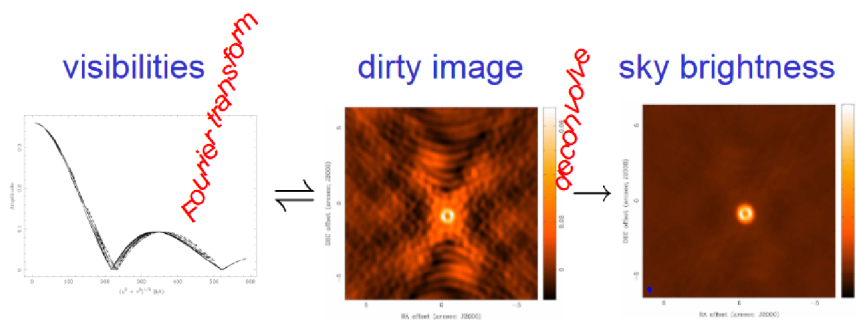


Figure 1.5: Fourier transform $I(u,v)$ samples to image plane to get $I_D(x,y)$ and then deconvolve $b(x,y)$ from $I_D(x,y)$ to determine (model of) $T(x,y)$.

1.2 Problems with real data - basics of calibration of interferometric measurement

In addition to incompleteness of our information due to the limited sampling in the uv space described above, there are other degradations of the signal because of imperfectness of the instrument and the influence of the Earth's atmosphere. In the range of mm/sub-mm wavelengths, which are dealt in this work, mainly the troposphere alters the passing signal due to water vapor and molecular oxygen.

There are three major effects of the atmosphere on the passing signal: (1) radio waves are absorbed (and therefore attenuated) before getting to antenna, (2) since a good absorber is also a good emitter, it adds lot of power noise, (3) the optical path makes time-dependent phase errors. The last effect is the most severe for radio/mm interferometry.

All these effects are increased with lower elevation of the observed object because of more air mass it has to go through. For the same reason, an altitude and humidity of the observatory plays important role. Because of that, the ALMA site has been chosen properly at alt. 5000 m and in the dry environment of the Atacama desert.

Joint effect of the noise contributed by our atmosphere's radiation and the instrument itself is characterised by *system power*, and, more frequently – thanks to the Rayleigh-Jeans law, by the *system temperature* T_{sys} . Similarly, the radiation coming from the (cosmic) source is characterised by the (equivalent) *antenna temperature*. For most of the radio sources from the deep Universe the $T_{sys} \gg T_{ant}$; our Sun is one of the rare exceptions.

Correction of the effects caused by the instrument and atmosphere is called *calibration*. It is based on observation of the objects, whose properties (e.g., total radio flux density, spectral distribution, position-and-shape) are known – so called calibrators. The atmospheric influence is also partly removed by observing in ONSOURCE and OFFSOURCE positions, once we have combined atmospheric and source signal, in the latter case solely the atmospheric contribution. The difference between the (ideal) calibrator model and its real observation is accumulated in so called *calibration tables*. And the same difference is then used for correction of the unknown source – our science goal. The calibration procedure has several steps (see below) and is accompanied also by selection of valid data. Because of technical imperfectness of the entire system, some data points are wrong (like in every measurement) and need to be discarded from further analysis. Usually, each data item has its bit-wise companion (true/false) called *flag* – the procedure of discarding the invalid data is then known as *flagging*. The data are flagged either automatically (e.g.,

the edge spectral channels with small sensitivity, data from antennas shadowed by another antenna) or based on a careful inspection of the data analysts (or specific SW – calibration pipeline). Typically, the wrong data shows up when we do diagnostic plots like phase or amplitude vs. frequency channel or time. Many calibration measurements are done before or during the observing sequence. The sequence containing calibration and science scans is called *scheduling block* (SB), and can be repeated several times, if needed by science goal (e.g., in order to increase sensitivity or – like with our Sun – to catch the internal dynamics of the observed object). Each repetition of a given SB is called *execution block* (EB).

Each EB starts with calibration of the antenna sensors for knowing our position on the sky, which we can accomplish by measuring known point source object that is close to our studied subject. In addition to that, the atmosphere (OFFSOURCE) scans are done. Next we need to find source with known radio flux density for the flux calibration. These calibrators are mostly quasars. Some frequency bandwidths of the instrument can be more sensitive than others or selective absorption of atmosphere can occur: This is eliminated by a scan that observes the source with a known spectrum – usually, again, some quasar, or a small bodies of the solar system (typically satellites of giant planets). Later, in course of the observation, the science-target scans interleave with the short scans of another close point source – the phase calibrator. As it has been already written – the phase variations, because of the atmospheric turbulence, can cause decoherence of the signal and therefore need to be corrected most frequently. Nowadays, the calibrations are mostly done in CASA (Common Astronomy Software Application) package. It is a software package govern by an international consortium of scientists based at the National Radio Astronomical Observatory (NRAO), the European Southern Observatory (ESO), the National Astronomical Observatory of Japan (NAOJ), the Academia Sinica Institute of Astronomy and Astrophysics (ASIAA), the CSIRO division for Astronomy and Space Science (CASS), and the Netherlands Institute for Radio Astronomy (ASTRON) under the guidance of NRAO. To the present day, it is the only officially supported system for interferometric and single-dish radio data done by ALMA or VLA. CASA replaced AIPS++, which was developed in early 90s as a substitution for AIPS. The core of the whole program are tasks and tools developed in C++ with user interface in Python, which enables to use these components.

CASA contains a lot of tools for processing interferometric and single-dish data and tools for specific telescopes. I will introduce only the main ones for calibration and some arguments with their function.

gencal()

General pre-calibration routine. With argument *tsys* it produces calibration table that describes the atmospheric and instrumental contribution to the total signal. It can be, e.g., also used for correction of antenna positions in the array (x,y, and z – with *antPos* as an argument).

setjy()

This task is used to set the proper flux density to the flux calibrator object and adjust thus the relative scale in voltages to absolute units in Jansky (Jy).

bandpass()

Bandpass task calculates a bandpass calibration solution, which means that it solves for gain variations in frequency.

gaincal()

Task *gaincal()* determines solutions for the time-based complex antenna gains, for each spectral window, from the specified calibration sources. Can solve both for amplitude and phase variations, separately or together.

aplycal()

The above CASA tasks make various calibration tables – it means they characterise the difference between idealized visibilities (calculated from the *models* of the calibrators) and their actually measured counterparts. The idea behind calibration postulates that the unknown studied object undergoes the same “distorsions” as the calibrators so that corrections in the form of “inversions” of the calibration tables can be applied also to the science target. This is realised by the CASA task *aplycal()*.

The calibration and flagging procedure finishes by making the *calibrated measurement set*. This already contains all possible corrections for influence of atmosphere and the instrument. Nevertheless, still we have only a sample of the visibilities $V(u, v)$ and we need to (i) make the IFT and (ii) iteratively deconvolve the instrumental PSF. Both of this procedures are unified in the CASA task.

tclean()

It allows to process the image from visibilities and deconvolve it. It is a new version of *clean()* and allows to process the imaging and deconvolution on parallelized computing methods. Thanks to its relative good performance it can be used also for *self-calibration loop*: A process where the unknown object itself is used as another phase calibrator and its model is iteratively improved (combining *gaincal('p')* and *tclean()*).

Processing of the solar data (see Section 2.2) basically follows this standard strategy, but in addition to it we have to (1) calculate the antenna temperature (because it can be in no case neglected w.r.t. the system temperature), and (2) put a correct celestial coordinates to the object at the Sun, based on the ephemeris submitted to the ALMA observing SW. We shall tackle the specifics of solar data processing briefly in Section 2.2.

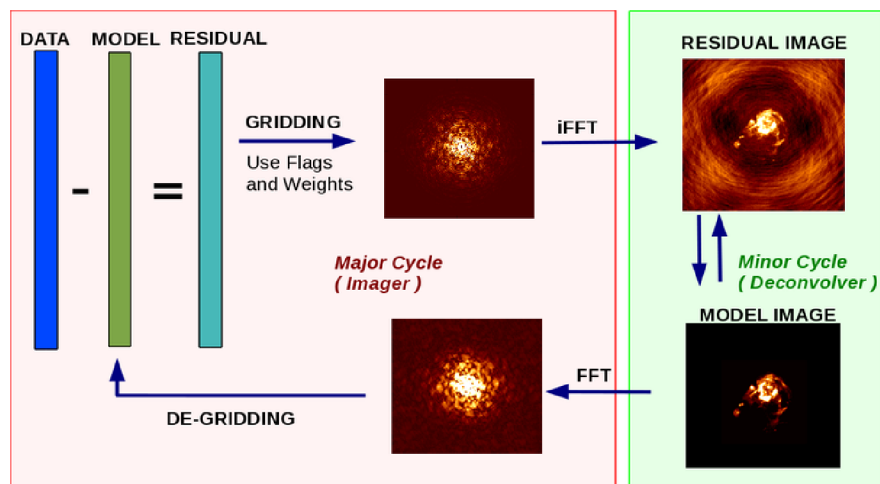


Figure 1.6: *tclean* procedure (*Task tclean description 2020*).

1.3 Modern interferometric observatories

As mentioned, radioastronomy is done by two ways, big single-dish telescopes or aperture synthesis with large arrays. The most straightforward and many times the most effective solution to our problem with resolution is huge parabolic refractors (single-dishes). Main advantage is direct view of the source and therefore abundance of artefacts. The bigger dish (measured in how many wavelengths we can fit in) the more precise our measurement is. Inspired by optical astronomy, radioastronomers are putting more detectors to focal point of the radiotelescope to make scanning more quicker. One of the examples is *multi-feed* detector *ALFA* with seven element on radiotelescope Arecibo in Puerto Rico ([Altschuler & Salter 2013](#)). Other advantage of single-dish systems is great sensitivity which comes with huge collecting area. This helps with detection of faint sources and spectral resolution - which comes hand in hand; Narrow spectral band means we need more photons.



Figure 1.7: The Arecibo Observatory in Puerto Rico ([Mario Roberto Durán Ortiz 2019](#)).

Building these enormous structures is good PR, but it has technical limits. Natural requirement is ability to steer and point on desired source, but these systems are also heavy and sensitive on wind, hence they are difficult to build. The biggest steerable radiotelescope is *Green Bank Observatory* (GBT), governed by American NSF, and German radiotelescope of Max Planck Society for radioastronomy in Effelsberg near Bonn, both with 100m main dish. It seems, for many reasons, we reached the peak of technical advancement in single-dish radioastronomy and no more progress is expected.

Different story is in sub- and millimetre wavelengths, which depends on precise shape of the dish. Thanks to technological advancements, we are able to build bigger and more precise dishes for this area than ever before. Good example is IRAM's (Institute Radio Astronomie Millimétrique) 30m dish in France near Grenobl, which played a part in global VLBI network EHT used for displaying black hole in M87. In this sense, 10m *South Pole Telescope* build in inhospitable Antarctic, played part too, adding a baseline. But the most famous progress in single-dish system is "Chinese Arecibo" - radiotelescope FAST (*Five hundred meter Aperture Spherical Telescope*) with diameter 500m (with effective collecting area 300m) so far the biggest single-dish telescope. Like Arecibo telescope,

they have limited steering options: (1) moving with detectors in focus plane, (2) partially changing geometry of the prime dish and (3) rotation of Earth itself. They also share the way they form spherical shape, they are build in a natural depression, but unlike FAST, telescope in Arecibo is also active radar; it is used for studying near-Earth asteroids. FAST's main scientific goals are study of pulsars, distribution of interstellar hydrogen on 1420MHz frequency and search after extraterrestrial civilizations SETI.

In radiointerferometry and aperture synthesis they try to evade technical difficulties of the single-dish by building more but smaller telescopes and combining their received signals. This idea was not new, but it lacked modern digital technology. There are many ways this can be done. The historically first was in construction of equidistant arrays of phase coordinated antennas, combined for better resolution in cross shape or in shape of letters "T" and "Y", for both direction of 2D sky sphere. Signal from waveguides is phase correlated and combined. It is the same concept as diffraction grating. This phased array behaves like one big telescope. The width of the main beam is also proportional to order λ/D , but here D does not mean diameter of antenna, but distance of the first and the last antenna. So why it is not enough to have only two antennas? Because we would have only thin beam, that would repeat every two periods of the beam and get indefinite image of the source; side lobes would be as big as the main one and we could not distinguish one from the other. Realization of interferometric antenna array with phase field can be done purely analogue and have been used since the 50s of 20. century. These arrays are easily distinguishable for their equidistant arrangement. Good example is radio interferometer in French Nancay or Siberian Solar Radio Telescope. This has also its weaknesses; we work with analogue frequency filters so the image is done for only finite (and rather small) number of discrete frequency channels with tight bandwidth (it does not contain spectral information, which is in astronomy very important). Because of these "defects" and technological advancements, we shifted on modern methods of aperture synthesis and interferometric systems with correlators, which these flaws do not have.

This list of interferometric system is only illustrative and contains systems that are focused or are able to do solar observations.

SSRT, which was already mentioned, is radioheliograph of the Institute of Solar-Terrestrial Physics in Irkutsk, Russia. Till recently, it work as two equidistant arrays in cross configuration in east-west and north-south directions. I mention it here again, because it is now under reconstruction for aperture synthesis system. They are changing the configuration of all 256 antennas and also it will have broader frequency range (Fig.1.8).

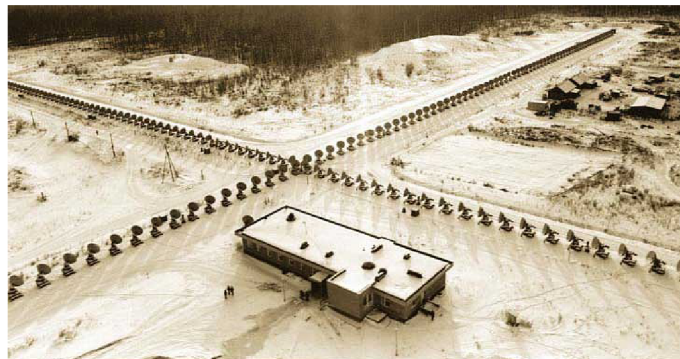


Figure 1.8: Siberian Solar Radio Telescope (example of X-shaped array) ([Sergey Trukhin 2015](#)).

MUSER (*Mingantu Spectral Radioheliograph*) is also system which is providing us radio maps of the Sun on multiple frequency channels; that will give us full spatial and spectral information of distribution of radio emission of the Sun. Thanks to strong signal from Sun and its variability, the instrument will have a solid time resolution. Users will have available dense array of 3D data cubes. MUSER is composed of two subsystems; low-frequency (400MHz- 2000MHz) with 40 parabolic antennas with diameter of 4,5 meters and high-frequency (2Ghz - 15GHz) with 60 2-meters also parabolic antennas. The maximum base for aperture synthesis is 3km, giving a 10" for the low-frequency and 1.4" for the high-frequency part.

GMRT (*Grand Meterwave Radio Telescope*) is a recently completed aperture synthesis interferometer operated by the National Institute of Radio Astrophysics (NACR TIFR) in Khodad near Pune, India. It does not have detailed spectral resolution, but it provides images at a total of six not very distant frequencies of 50, 153, 233, 325, 610 and 1420 MHz in the wavelength meter range. This covers the area quite well. The longest base is 25km, providing a limit resolution of 2" at 1.42GHz. The instrument is not dedicated to solar observation, but is sometimes used to observe the sun.

LOFAR (*LOw Frequency ARray*) is enormous interferometer working on relatively long radio waves in range of frequencies 10MHz - 240MHz. It was built by an international consortium of European countries and its antennas are located in almost the whole of Western and Central Europe, on an area whose linear dimensions exceed 1000 km (Fig.1.9). The device provides very long bases and works on the VLBI principle. LOFAR synchronization at remote stations is performed using dedicated broadband Internet connections. However, this system is used for communication between distant antennas (that is, for long bases that provide Fourier components for short scales in the image), the "nests" of the antennas at each station have much shorter bases (thus displaying medium and long-range radio source scales) and are interconnected by standard waveguides. Although the primary objective of the instrument is not the observation of the Sun, one of the six key scientific areas covered by the LOFAR project is called "Solar Physics and Space Weather".



Figure 1.9: Locations of the International LOFAR Telescope ([ASTRON 2018](#)).

NOEMA (*Northern Extended Millimetre Array*) is built and operated by the Institute of Millimeter Radio Astronomy (IRAM) in Grenoble, France (this is a joint project of the French CNRS, the German MPG and the Spanish IGN). The observatory itself is located at Plateau-du-Bure in the French Alps. It is a lively, ever-expanding project - at present it is equipped with twelve 15m antennas placed on the railway track, allowing variable configuration of the whole field with the largest base 1.6km. It observes the northern sky (thus complementing the area unreachable from ALMA) in mm wavelengths from 70GHz to 370GHz.

(E)VLA (*Expanded Very Large Array*) is an interferometer in American New Mexico, undergoing extensive modernization (VLA \rightarrow EVLA). It operates in the 1GHz - 50GHz band, perfectly complementing the LOFAR low-frequency field observation and the ALMA high-frequency observatory. The (E) VLA antennas, along with nine other radio telescopes in the US, can cooperate within VLBI interferometry, and the whole system is called VLBA (Very LongBaseline Array).

SKA (*Square Kilometre Array*) is still project of the future. This international project, if implemented, will not bring the first scientific data until 2023, but its full completion is planned for 2030. However, after experience building the ALMA observatory, it can be safely said that a gigantic project is likely to lead to some delay - which is rather normal in pioneering projects deploying unproven new technology. In addition to the unimaginable sensitivity of the instrument given by the total effective collection area of the antenna of approximately 1 km^2 (hence the name of the instrument), the SKA observatory would reach unprecedented resolution as its antennas are to be deployed in two continents, South Africa and Australia and New Zealand. Therefore, the use of VLBI technology for correlation between continental antennas is a matter of course. In this case, the atomic clock should provide the necessary synchronization. The SKA should cover a relatively large and continuous frequency range from 50MHz to 14GHz (with a plan to expand to 30GHz). Because the ideal antenna parameters change in such a wide interval, the whole array will be implemented as two subsystems for long and medium + short wavelengths (+ additional smaller survey array). Even in this case, the primary objective is not the observation of the Sun, but one of the scientific programs called "Cosmic Magnetism" implicitly counts on research into the magnetic fields of the Sun by this device (Czech solar radio astronomers are involved in the relevant international working group). If this project is fully implemented, it is likely to revolutionize astrophysics. The SKA field already has smaller "opening projects" to test technologies designed to be used on a larger scale on SKA - the MeerKAT interferometric systems in South Africa and the MWA (Murchinson Widefield Array) in Australia.

ALMA (*Atacama Large Millimetre/submillimetre Array*) is a project of interferometric system for receiving radio waves of millimetre and submillimetre lengths, covering an area of almost 200 km^2 . It is built and operated by the joint efforts of the European Southern Observatory (ESO), the American National Radio Astronomy Observatory (NRAO) and the Japanese National Astronomical Observatories of Japan (NAOJ) in the Atacama Desert, Chile, at 5,000 meters above sea level so the Earth's atmosphere gases (especially in water vapor) interfere with observation as little as possible. It has become a key instrument in astrophysical research for at least the next decade. ALMA is able to study the first stars and galaxies from the cosmic "dark ages", billions of years ago. Or even the nearby Universe, ALMA provides an unprecedented ability to study the processes of star and galaxy formation. Unimpeded by the dust that obscures visible light observations, ALMA can reveal the details of young, still-forming stars and show young planets still in

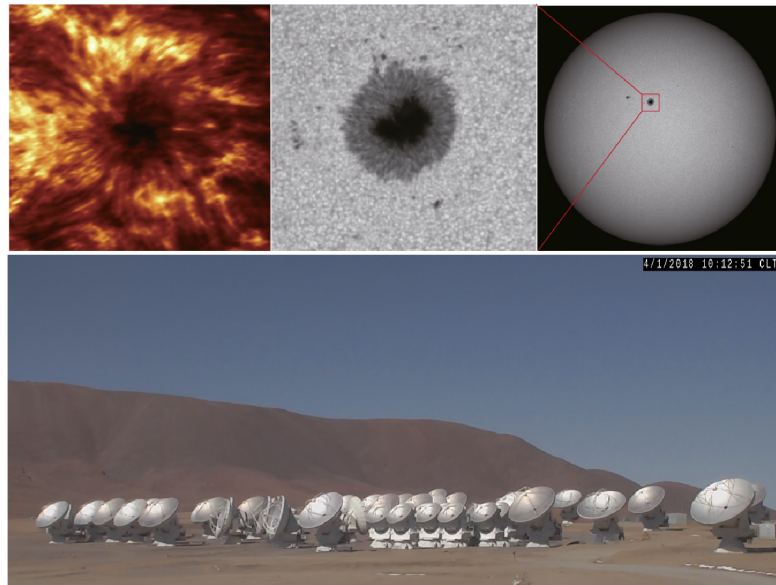


Figure 1.10: ALMA and sample of data (courtesy of M.Bárta).

the process of development. the objects of the distant universe and our cosmic vicinity, for which the telescope was primarily designed, it is now engaged in research into our closest star, the Sun. In many respects, ALMA is launching a new era in observational astronomy. It not only opens up a completely new observation window in the THz frequency range, it also provides unprecedented spatial and frequency resolution in two independent polarizations, and has an unprecedented sensitivity thanks to its large total collection area. Since 2013 ALMA is officially in full operation.

Because the Sun is much different than usual cosmic target ALMA has, (stronger radio source, bigger diameter than the arrays field of view, overheating of the receivers), special observation mode was developed. It is since 2017 used for research and perfectly going. With new understanding of ALMA's capabilities more research is done, ALMA has already over 1500 scientific publications and 1800 proposals for observations with ALMA are received on average each year.

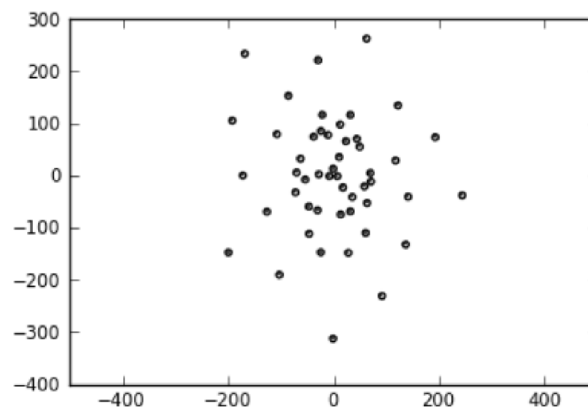


Figure 1.11: ALMA array in one of its compact configurations (Bárta 2016).

2. Solar research with ALMA

2.1 What can ALMA tell us about the Sun

Both for other areas of astrophysics and solar physics, ALMA will solve many long-standing questions. One of them is particle acceleration in solar flares, which we know not only from radio-spectroscopy but from Hard X-rays (HXR); it's high intensity is nowadays used for detection of eruption activity. Thanks to HXR we know the energy and quantity of these particles, but our 'standard' model tells that there are too much of them to be only accelerated by electric field. There are many theories of the origin but preliminary calculations are suggesting that these accelerated electron beams can, thanks to interaction with magnetic field, radiate with gyrosynchrotron mechanism. With this kind of emission and due to high energy, the wavelengths fall onto millimeter and sub-millimeter range, which with ALMA's great spatial resolution gives us hope to have direct measurement of these beams and maybe even regions where they come from.

Other unsolved question is convection in Sun and other stars. Numerical calculations are giving us detailed picture of convection in upper layer of photosphere and chromosphere but we lack observations that would confirm these models or even give us some calibration parameters. One of the numerical models gives us detailed temperature structure of the chromosphere, but comparison with optical and especially spectroscopic measurements is problematic due to calculation of the temperature. To get the model of spectral line we need to solve equations of radiation transmission, but we can do that only if the transmission is in thermal equilibrium. If we would try to solve inverse problem, that is, try to get parameters (temperature, ...) from spectral lines of the plasma, there would be ambiguity and beside that, optical observations do not have the spatial resolution yet to distinguish lines from convective cells. On the other hand, observation of thermal radiation of lower chromosphere and photosphere (which falls in millimeter range) by ALMA can measure the temperature directly and with amazing spatial resolution. Thanks to that, ALMA is able to give us answers to understanding of temperature structure of chromosphere and surface convection on Sun.

Similar problem is with fine structures of solar protuberances. They are made of chromospheric material, which are maintained by magnetic field in heights corresponding to the corona. With every new solar probe we get more details of the fine structure of protuberances, which lead us to more questions, especially about their dynamics (Fig. 2.1). ALMA has far greater resolution than these probes so it is able to examine all scales of assumed filamentation of the material in the protuberance up to the level of the dissipation scale. Apart from that, in the calm chromosphere, thermal radiation of protuberances and optical observations could separate effects of density and temperature on intensity of emission and directly get temperature and density structure of protuberances.

With ALMA we have possibility to study recombination spectral lines formed by elec-

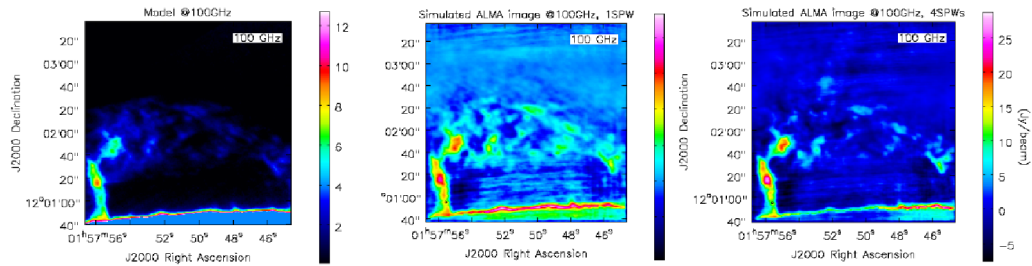


Figure 2.1: Simulation of solar protuberance done in CASA (Heinzel et al. 2015).

tron transitions between high levels of a hydrogen atom. Its existence was not yet confirmed, but if they are there, it would give us important diagnostic tool for measurement of magnetic fields in the part of the solar atmosphere where it is otherwise difficult or impossible.

2.2 How can we make ALMA observing the Sun

As the solar physicists are getting to know the possibilities of ALMA, many more questions are revealing themselves with an opportunity to be answered with data from ALMA. They build and constructed it to be able to observe the Sun, but it was a long way to get the right data. They had to make sure that when pointing to Sun, radiation would not damage the receivers because Sun is much more stronger radio source than usual ALMA scientific targets in distant universe. So the specific Solar Observing Mode was developed. E.g. the luminance temperature in the chromosphere corresponds to the kinetic temperature of the chromospheric plasma and is therefore of the order of 10000K. But ALMA is sensible enough to register radio sources with luminance temperature tenth of Kelvin. Unfortunately, no detector is able to handle this dynamic range of intensity (and have linear characteristic). Because ALMA's advantage is high sensitivity and the detector has linear sensitivity for low intensities but for luminance temperatures around 5000K saturation occurs. So they came up with attenuators, filters that can be placed before the receivers, when expected high intensity to be measured. Yagoubov (2013b, 2014) remarked that ALMA SIS mixers could be debiased to reduce the mixer gain and effectively increase the saturation level to a degree that allows solar observations without the use of the solar filters, at least for non-flaring conditions on the Sun. These produce lower conversion gain and since the dynamic range scales roughly inversely with gain, these settings can handle larger signal levels before saturating. Other problem is with overheating of detectors. Fortunately, they thought about this problem in the beginning and made the antennas so that for visible and infrared radiation the surface would look rough and dispersive but leave it coherent for millimeter and sub-millimeter wavelengths.

The field of view of both 7-m and 12-m ALMA antennas is smaller than diameter of the Sun, therefore the array is insensitive to solar background. This can be fixed by fast-scan mapping the whole Sun disk. It recovers information about absolute temperature, large spatial scales in mosaic images and minimizes the impact of atmospheric variation. In the end, you have the whole solar disk map in 7 minutes and it can be useful for studies of limb brightening and for distinguishing between various solar atmospheric models. Nowa-

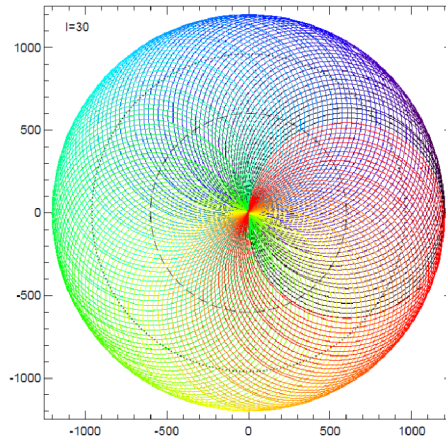


Figure 2.2: Double-circle single-dish scanning pattern. Consecutive minor circles which denote the actual path of the antenna are coloured. Inner dashed circle denotes the major circle around which minor circles move. Dotted circle represents the solar disk. Units are given in arcseconds (White et al. 2017).

days is used double-circle fast-scan. An advantage of this type of mapping is that antenna moves steadily with constant velocity throughout the target, there are no sharp turns or accelerations and its coverage matches the shape of the solar disk and it repeatedly revisits the region of the center of the disk, allowing atmospheric opacity variations to be corrected.

Sun is ever-changing object; it changes in course of the day (differential rotation) or even seconds (flares and eruptions). One of the problem is that we do not have enough samples in the u - v plane and we can not use the rotation of the Earth when observing quickly changing regions. Fortunately, there were developed simulation functions in *CASA* for finding the optimal mode for observing individual science cases. `simobserve()` can generate visibilities and `simanalyze()` produces a cleaned image based of these visibilities and generate diagnostic image. Other problem is trying to track the specific solar target. In order to do that, we need to know Sun's physical ephemeris, offsets relative to physical ephemeris and its rotation. This can be provided by ALMA solar ephemeris generator - based on the Jet Propulsion Laboratory (JPL) Horizon web interface. Solar observer can specify the target offset relative to center of the Sun and use a model to correct for the Sun's differential rotation. Ultimately you get a targets coordinates as a function of time.

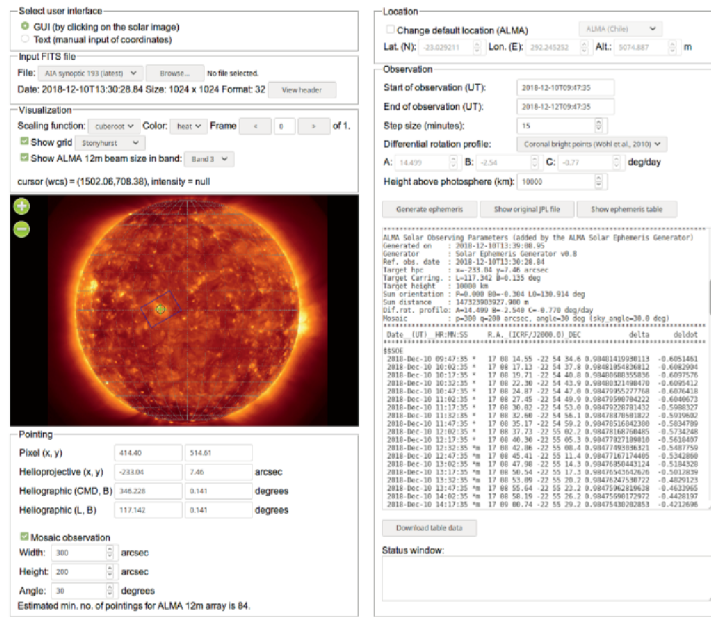


Figure 2.3: The ALMA Solar Ephemeris Generator user interface (Skokić & Brajša 2019).

When we have the right configuration for the observation and we get the final calibrated data from CASA, which will be discussed how in next chapter, we get FITS file with luminance temperature of solar atmosphere for reference time in heliocentric equatorial coordinates, right ascension α and declination δ . These coordinates are inconvenient for further work. E.g. impossibility to compare the data with data from other solar observatories like SST, Gregor or probes Hinode or SDO (and others...), because they work with Helioprojective Coordinates (Fig. 2.4). Part of this thesis is to make script for this conversion and test it by composition with data from SDO and its instruments.

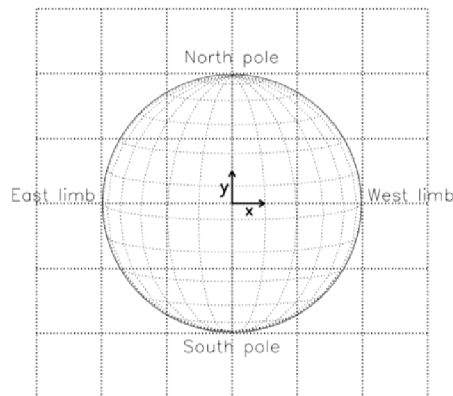


Figure 2.4: Heliographic and helioprojective coordinate systems (White et al. 2017).

3. Procedure for the transformation of solar data from the ALMA observatory: own contribution to the scientific use of solar observations

In spite I cannot use the solar data from my own project (from the submission of the proposal for observing time to receiving the calibrated data it usually takes more than a year), a lot of solar observations are available in the [ALMA Science archive \(2020\)](#). The science data are protected for the project PI for one year, than they become publicly available. I have used this opportunity. Moreover, the data taken during Commissioning & Science Verification of the Solar ALMA Observing Mode are freely available too.

In order to demonstrate that the procedure, which transforms the final ALMA FITS image into the appropriate HPC coordinates (and which is the main practical goal and outcome of thesis) works well, we would like to compare (overlay) the solar ALMA images with their counterparts observed in optical or UV/EUV radiation. Therefore, the data containing significant structures visible both in optical or UV telescopes and ALMA, have been selected.

We started with a raw, uncalibrated data and basically followed the procedure as described in the *CASA Guide* for solar ALMA CSV data ([CASA Guide 2018](#)). The observation used in the *CASA Guide* is a mosaic of the large sunspot, hence, a suitable structure for the comparison with its optical counterpart. The data are available either via ALMA Archive or through the link in the above mentioned tutorial.

After I download and unpack the data in terminal:

```
1 tar -xvzf Sunspot_Band6_UncalibratedData.tgz
2 cd Sunspot_Band6_UncalibratedData
```

And import some scripts:

```
1 import analysisUtils as aU
2 es = aU.stuffForScienceDataReduction()
3 execfile('Sun_reduction_util.py')
```

I can go to CASA, which the following code will be in. First i define the directory name of the ALMA Science Data Model (ASDM) and some directory names of the Measurement Sets (MS) for the calibration:

```
1 asdm = 'uid___A002_Xae00c5_X2a8d'
2 mso = asdm + '.ms'
```

```

3 mss = asdm + '_split.ms'
4 msc = mss + '.cal'

```

Before I can work with the data, I need to convert them into CASA MS format, which is simply done by task `importasdm`. Row 2. and 3. are for correction of SYSCAL table times.

```

1 importasdm(asdm = asdm, vis = mso, asis='Antenna Station Receiver Source
    CalAtmosphere CalWVR CorrelatorMode SBSummary CalDevice ')
2 from recipes.almahelpers import fixsyscaltimes
3 fixsyscaltimes(vis = mso)

```

First step will be getting to know what is in the data. That is done by task `listobs`:

```

1 listobs(mso, listfile = asdm + '_listobs.txt')

```

I will now show this text file here, but it can be found on the attached link. My main focus is on first and third sections. The scientific observations are done with the spectrum windows (Spw) 0 12, and the IDs of the Spw with 128 channels, which are used for image synthesis, are 5, 7, 9, and 11. Therefore, we will calibrate the data of SpwID 5, 7, 9, and 11 only. The data of spwID 0, 1, 2, 3 are the data from the square-law detectors of the basebands. The data will be used for creating Tsys+Tant (Temperature of system + Temperature of antenna) tables, and are archived as the auto-correlation data in the dataset.

Some scans in the data were used by the online system for pointing and sideband ratio calibration. These scans are no longer needed, same as the averaged data of each Spw, so I flag them `flagdata` by selecting on 'intent'(1. and 2. row), then saving current flagging state using the `flagmanager` task (3. row).

```

1 flagdata(vis = mso, mode = 'manual', intent = '*POINTING*,*SIDEBAND_RATIO*'
    , flagbackup = False)
2 flagdata(vis = mso, mode = 'manual', spw = '6,8,10,12', flagbackup = False)
3 flagmanager(vis = mso, mode = 'save', versionname = 'priori1')

```

Now I calibrate the data by Tsys, which gives a first-order correction for the atmospheric opacity as a function of time and frequency, and associates weights with each visibility that persist through imaging. The data contain Tsys measurements, so by task `gencal` I generate the calibration table.

```

1 gencal(vis = mso, caltable = mso + '.tsys', caltype = 'tsys')
2 flagdata(vis = mso + '.tsys', mode = 'manual', spw = '
    5:0~9;116~127,7:0~9;116~127,9:0~9;116~127,11:0~9;116~127', flagbackup =
    False)
3 es.checkCalTable(mso+'.tsys', msName=mso, interactive=False)

```

Now I apply the the Tsys calibration on bandpass calibrator using the task `applycal`, which reads the specified gain calibration tables, applies them to the (raw) data column, and writes the calibrated results into the corrected column.

```

1 applycal(vis = mso, field = '1', spw = '5,7,9,11', gaintable = mso + '.tsys
    ', gainfield = '1', interp = 'linear,linear', calwt = True, flagbackup =
    False)

```

I also need to calibrate the phase calibrator:

```

1 applycal(vis = mso, field = '2', spw = '5,7,9,11', gaintable = mso + '.tsys
    ', gainfield = '2', interp = 'linear,linear', calwt = True, flagbackup =
    False)

```

The standard method of Tsys calibration cannot be apply to the data of the Sun, because the antenna temperature of the Sun cannot be neglected for estimating the system equivalent flux density (SEFD). To estimate correct SEFD at the Sun, the solar observing sequence includes some special measurements, like the measurement of zero-signal level. The subroutines for creating and applying Tsys+Tant calibration tables are prepared by the ALMA solar development team. For the Tsys+Tant calibration of the solar data, you will execute only the following command:

```
1 sol_ampcal_2(mso, mso + '.tsys', exisTbl=False, outCSV=True)
```

Since I completed the Tsys and Tsys+Tant calibration, the data that are not used in the image synthesis are flagged. The data are: auto-correlation and atmosphere calibration (1. and 2. row), spectral windows that are not used (3. and 4. row), the channels near the both edges of the spectrum window (10 channels) (5. row):

```
1 flagdata(vis = mso, mode = 'manual', autocorr = True, flagbackup = False)
2 flagdata(vis = mso, mode = 'manual', intent = '*ATMOSPHERE*', flagbackup =
  False)
3 flagdata(vis = mso, mode = 'manual', spw = '0~4', flagbackup = False)
4 flagdata(vis = mso, mode = 'manual', spw = '13~36', flagbackup = False)
5 flagdata(vis = mso, mode = 'manual', flagbackup = False, spw='
  5:0~9;116~127,7:0~9;116~127,9:0~9;116~127,11:0~9;116~127') ;
```

The some sub-scans at the start and end of the scientific scans are used to measure the sky with the setting of optimized for the Sun. Since the data are used only for estimating the antenna temperatures at the Sun, I flag the data:

```
1 mymsmd = createCasaTool(msmdtool)
2 mymsmd.open(mso)
3 sciScan = mymsmd.scansforintent('*OBSERVE_TARGET*')
4 mymsmd.done()
5 for i in range(0, len(sciScan)): \label{\label{\label{\label{{\tiny key}}}}}}
6 subInf=aU.computeDurationOfScan(sciScan[i], vis=mso, returnSubscanTimes=
  True)
7 subNum = subInf[1]
8 flagdata(vis = mso, timerange = subInf[3][1], mode = 'manual', flagbackup =
  False)
9 flagdata(vis = mso, timerange = subInf[3][2], mode = 'manual', flagbackup =
  False)
10 flagdata(vis = mso, timerange = subInf[3][subNum-1], mode = 'manual',
  flagbackup = False)
11 flagdata(vis = mso, timerange = subInf[3][subNum], mode = 'manual',
  flagbackup = False)
```

As we can see from the text file with data information, the Tsys values of DA54 antennas are significantly large. Therefore, I flag the data of the antenna and save the flagging state:

```
1 flagdata(vis = mso, antenna = 'DA54', mode = 'manual', flagbackup = False)
2 flagmanager(vis = mso, mode = 'save', versionname = 'priori2')
```

For flux calibration was used quasar nrao350. I obtained the flux density and spectral index of the nrao350 from the ALMA calibrator database (1. - 9. row) and fill the model data column for nrao350 with a model (10. row):

```
1 intentSources=es.getIntentsAndSourceNames(mss)
2 ampCalId = intentSources['CALIBRATE_AMPLI']['id'] + intentSources['
  CALIBRATE_FLUX']['id']
3 calFieldNames = intentSources['CALIBRATE_AMPLI']['name'] + intentSources['
  CALIBRATE_FLUX']['name']
4 amp_cal_name=calFieldNames[1]
```

```

5 spwInfo=es.getSpwInfo(mss)
6 obs_freq="%fGHz"%(spwInfo[0]['refFreq']/1e9)
7 date=aU.getObservationStartDate(mss)
8 date_obs=date.split()[0]
9 spw1_flux=aU.getALMAFlux(sourcename=amp_cal_name, date=date_obs,frequency=
  obs_freq)
10 setjy(vis = mss, field = '2', spw = '0,1,2,3', standard = 'manual',
  fluxdensity = [spw1_flux['fluxDensity'], 0, 0, 0], spix= spw1_flux['
  spectralIndex'], reffreq = obs_freq)

```

After that, I determine the reference antenna (1. row) and run the task gaincal on the bandpass calibrator to determine phase-only gain solutions. I used solint='int' for the solution interval, which means that one gain solution will be determined for every integration time (2. row) and if it looks correct (you can check with 3. and 5. row), create the bandpass calibration table (4. row):

```

1 ref_ant = 'DA41'
2 gaincal(vis = mss, caltable = mss + '.ap_pre_bandpass', field = '1', scan =
  '5', solint = 'int', refant = ref_ant, calmode = 'p')
3 es.checkCalTable(mss+'.ap_pre_bandpass', msName=mss, interactive=False)
4 bandpass(vis = mss, caltable = mss+'.bandpass', field = '1', scan = '5',
  solint = 'inf', refant = ref_ant, solnorm = True, bandtype = 'B',
  gaintable = mss+'.ap_pre_bandpass')
5 es.checkCalTable(mss+'.ap_pre_bandpass', msName=mss, interactive=False)

```

Using the bandpass calibration table and solint='int' option, I determine phase-only gain solutions of the calibrators:

```

1 gaincal(vis = mss, caltable = mss + '.phase_int', field = '1~2', solint = '
  int', refant = ref_ant, gaintype = 'G', calmode = 'p', minsnr = 3.0,
  gaintable = mss + '.bandpass')

```

For amplitude-only gain solutions on the scan time, I use the bandpass and phase calibration tables:

```

1 gaincal(vis = mss, caltable = mss + '.ampli_inf', field = '1~2', solint = '
  inf', refant = ref_ant, gaintype = 'G', calmode = 'a', minsnr = 3.0,
  gaintable = [mss + '.bandpass', mss + '.phase_int'])

```

I will now derive the flux density of the other calibrators by using the flux calibrator (whose flux density was set in setjy above):

```

1 fluxscaleDict = fluxscale(vis = mss, caltable = mss + '.ampli_inf',
  fluxtable = mss + '.flux_inf', reference = '2')
2 es.fluxscale2(caltable = mss+'.ampli_inf', removeOutliers=True, msName=mss,
  writeToFile=True, preavg=10000)

```

Now I can create the gain calibration table of phase-only gain solutions on the scan time:

```

1 gaincal(vis = mss, caltable = mss+'.phase_inf', field = '1~2', solint = '
  inf', refant = ref_ant, gaintype = 'G', calmode = 'p', minsnr = 3.0,
  gaintable = mss+'.bandpass')

```

When I have all the calibration tables I can apply them on the bandpass, flux and phase calibrators (1. and 2. row) and then on solar data (3. row):

```

1 for i in ['1', '2']:
2 applycal(vis = mss, field = str(i), gaintable = [mss + '.bandpass', mss+'.
  phase_int', mss+'.flux_inf'], gainfield = ['', i, i], interp = 'linear,
  linear', calwt = True, flagbackup = False)

```

```

3 applycal(vis = msc, field = '0, 3~150', gaintable = [mss+'.bandpass', mss+'.
  .phase_inf', mss+'.flux_inf'], gainfield = ['', '2', ''], interp = '
  linear, linear', calwt = True, flagbackup = False)

```

With calibrations all done, I can split out the CORRECTED data column:

```

1 split(vis = msc, outputvis = msc, datacolumn = 'corrected', keepflags =
  True)

```

Last but not least, we have to attribute the image correct RA/Dec coordinates. During most solar observations, the antennas are tracking a structure on the Sun according to the solar differential rotation (and daily motion on the sky), so the image frame is fixed on the solar frame, but the frame is moving on the RA/Dec coordinate frame. Basically, the FIELD table (a part of the Measurement Set) for the ephemeris objects contains a reference field with coordinates [0,0] and the other fields of the mosaic are described just as an offset to this *phase reference* direction. We need to recalculate the coordinate of each field. First, I modify the coordinate of the (reference) field “0” from the reference time using `fixplanets()` task. The reference time has to be the time when the antennas are directed to the field “0” (1. and 2. row). Then we basically add the original offsets to the newly defined absolute coordinates, first rescaled from radians to arc seconds (3. to last row):

```

1 tb.open(msc+'/FIELD', nomodify=True)
2 phsCenOff = tb.getcol("PHASE_DIR")
3 tb.close()
4 refRaDec = aU.rad2radec(phsCenOff[0][0][0], phsCenOff[1][0][0], prec=1,
  hmsdms=True, delimiter=' ')
5 for i in range(3, 151):
6 raOff = phsCenOff[0][0][i] * 180./pi * 60. *60.
7 deOff = phsCenOff[1][0][i] * 180./pi * 60. *60.
8 offRaDec = aU.radec2deg(aU.radecOffsetToRadec(refRaDec, raOff, deOff, prec
  =1))
9 offRaDecF = 'J2000 ' + aU.deg2radec(offRaDec[0], offRaDec[1], prec=1,
  hmsdms=True, delimiter=' ')
10 fixplanets(msc, field =str(i), fixuvw = False, direction = offRaDecF)
11 tb.open(msc+'/FIELD', nomodify=False)
12 tgt_refdir = tb.getcol("RefDir_Ref")
13 for id in range(3, len(tgt_refdir)):
14 tb.putcell("RefDir_Ref", id, 21)
15 tb.putcell("DelayDir_Ref", id, 21)
16 tb.putcell("PhaseDir_Ref", id, 21)
17 tb.close()

```

In addition, the direction in the pointing table has a bad influence to the coordinate system of the image synthesis, which I will do next, so I erase it:

```

1 tb.open(msc+'/POINTING', nomodify = False)
2 a = tb.rownumbers()
3 tb.removerows(a)

```

In this observation the actual duration of the observations does not exactly equal to the required duration of the 149-pointing MOSAIC. Some fields were observed twice, but even though the scans are valid, for keeping the uniformity of the sensitivity in a map, it is better that they are not used for the image synthesis:

```

1 msc = "uid__A002_Xae00c5_X2a8d_split.ms.cal"
2 flagdata(vis = msc, mode = 'manual', timerange = '
  2015/12/18/20:02:35~20:08:20', flagbackup = False)

```

Now I have everything ready to synthesize a sunspot image from the visibilities, so I use clean task:

```

1 clean(vis = msc, spw = '0,1,2,3', stokes = 'I', field='0,3~150', phasecenter
   = '0', imagename='AR12470_B6AllSpw_I', cell = '0.15 arcsec', imsize =
   [2048, 2048], interactive = False, mask = 'box [[555pix,565pix],[1505pix
   ,1490pix]]', weighting = 'briggs', robust = 1., niter = 5000000000,
   psfmode = 'clark', imagermode='mosaic', mosweight = True, minpb=0.3,
   pbcor=False, threshold='1.0Jy', gain=0.1)

```

Finally, I do the primary beam correction and create the FITS file of the corrected map:

```

1 impbcor(imagename='AR12470_B6AllSpw_I.image', pbimage='AR12470_B6AllSpw_I.
   flux', outfile='AR12470_B6AllSpw_I.pbcor', mode='divide')
2 exportfits(imagename='AR12470_B6AllSpw_I.pbcor', fitsimage='
   AR12470_B6AllSpw_I.fits')

```

And that is it from CASA, now comes the Python script for converting the coordinates. First of all, we need to open the FITS file and extract the data and the header.

```

1 def loadFits(self):
2     hdu = fits.open(self.file_)
3     hdr = hdu[0].header
4     im = hdu[0].data[0,0]
5     return hdu, hdr, im

```

Then, get the coordinates and observation time from header.

```

1 obstime = self.hdr['DATE-OBS']
2 self.obstime = Time.Time(obstime)
3 ra = radians(self.hdr['crval1'])
4 dec = radians(self.hdr['crval2'])

```

Here I define a function where input are heliocentric equatorial coordinates (HEQ) and output are helioprojective coordinates (HPC). Unfortunately, there is not a right and easy way to convert them, so I needed to convert them to Horizontal coordinate system (AltAz) and then to HPC. I also needed location of the observer and distance of the Sun in the time of observation (2. and 3. row). Now the comes the conversion itself. First we change coordinates values to type which we can work with (4. and 7. row). Next I prepare a frame of the AltAz coordinates (5. row). Now the conversion happens (6. and 8. row). Last row returns these values.

```

1 def radec2hpc(self, ra, de):
2     alma = EarthLocation.of_site('ALMA')
3     distance = sunpy.coordinates.sun.earth_distance(self.obstime)
4     c_rd = SkyCoord(ra=ra*u.rad, dec=de*u.rad, frame='icrs', obstime=self.
       obstime)
5     frame = AltAz(obstime=self.obstime, location=alma)
6     temp = c_rd.transform_to(frame)
7     sun_altaz = SkyCoord(az=temp.T.az, alt=temp.T.alt, distance=distance, frame
       =frame)
8     sun_hp = sun_altaz.transform_to(frames.Helioprojective)
9     return sun_hp.T.Tx.value, sun_hp.T.Ty.value

```

After we get HP coordinates we write them to header.

```

1 crval1, crval2 = self.radec2hpc(ra, dec)
2 self.hdr['crval1'] = crval1
3 self.hdr['crval2'] = crval2

```

HEQ and HP coordinates are rotated by solar angle P to each other, so the data have to be rotated too. First I copy the header (2. row) and change some keywords (3. - 9. row) to be coherent with new coordinates. From sunpy library I called the solar angle (10. row), rotate the data by it (11. row) and return the data and the new header (12. row).

```

1 def RotationOfMap(self):
2     hdr_n = self.hdr.copy()
3     hdr_n['cdelt1'] = abs(self.hdr['cdelt1']*3600)
4     hdr_n['cdelt2'] = abs(self.hdr['cdelt2']*3600)
5     hdr_n['ctype1'] = 'HPLN-TAN'
6     hdr_n['ctype2'] = 'HPLT-TAN'
7     hdr_n['cunit1'] = 'arcsec'
8     hdr_n['cunit2'] = 'arcsec'
9     del(hdr_n['comment'])
10    sun_eph_P = sunpy.coordinates.sun.P(self.obstime)
11    rota = scipy.ndimage.rotate(self.im,angle = sun_eph_P.degree ,order=4,
12                                prefilter=False,reshape=False , cval=np.nan)
13    return rota,hdr_n

```

Now I have the data and header (1. row), I save it to a FITS file.

```

1 rota,hdr_n = self.RotationOfMap()
2 sunpy.io.fits.write('HPC'+self.file_, rota , hdr_n)

```

So now, I will use this Python code on FITS file I got from CASA (Fig.3.1).

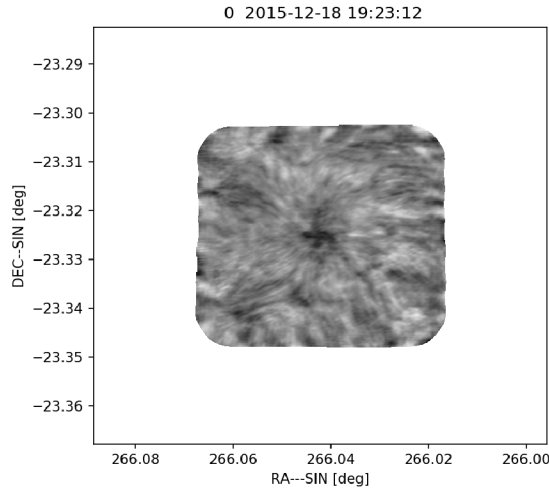


Figure 3.1: Data from CASA.

Keyword	
CRVAL1	2.660E+02
CDELTA1	4.167E-05
CRVAL2	-2.332E+01
CDELTA2	4.167E-05
DATE-OBS	2015-12-18 19:23:12.720

Table 3.1: Data from header.

Here is the data after running through the code with comparison to data from Helioseismic and Magnetic Imager from SDO probe.

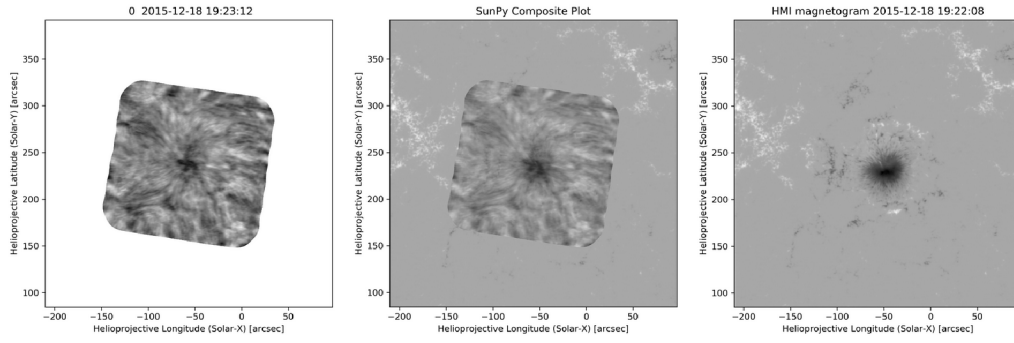


Figure 3.2: Processed data compared to data from SDO/HMI.

Keyword	
CRVAL1	-106.576
CDELTA1	4.167
CRVAL2	238.167
CDELTA2	4.167

Table 3.2: Data from new header.

In addition to the sunspot I have processed another dataset – observation of a small solar prominence. Advantage of this dataset is in the fact that it contains the solar limb, whose position can be quite exactly co-aligned and compared with the other data. In this case, I have been using another instrument at the SDO – AIA, which 'looks' to same part of Sun's atmosphere in EUV line:

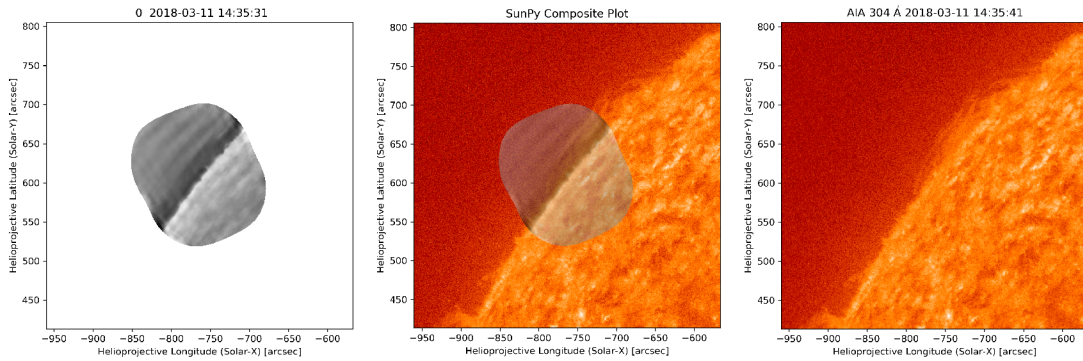


Figure 3.3: Processed data compared to data from SDO/AIA.

Here (Fig. 3.3), we can see that the edge fits nicely too. It is not precise (uncertainty of 4 pixels and can even have error of wrong correction on bending of light in general relativity), but enough to distinguish same solar structure or filaments.

Conclusion

Once again, I would like to point out how the data from ALMA are helpful for solar research and millimeter and sub-millimeter research in general. Thanks to ALMA we are able to study parts of the Sun with unprecedented details (have 10 times more details than Hubble Space Telescope) and incredible resolution (10 milliarcseconds maximum angular resolution (equivalent to a basketball hoop on the Moon)). With this unprecedented spatial resolution we are able to study convection of stars in upper of photosphere and chromosphere and fine structures of solar protuberances. Maybe even discover recombination spectral lines formed by electron transitions between high levels of a hydrogen atom. These are just some examples of problem related to studying our Sun, but ALMA is able to solve many and more yet unsolved question in other fields of astrophysics.

Studied solar activity never happens on one frequency or in one part of Sun's atmospheres, so we also rely on many other telescopes and/or probes. But because ALMA does not work only on solar research, observations are made in standard equatorial coordinates, therefore solar physicists are unable to process the data further. So there is a need for a script that would convert these coordinates for further data analysis with other solar observations or even for checking the pointing of ALMA. This would enable 90% solar physicist to access the data and use them to their own will.

This script is rather simple, from FITS file I got from CASA, I used the observation time and coordinates of the center pixel (the scaling is the same for both datasets) and through sunpy and astropy libraries, I converted the coordinates and rotated the map by solar angle P. Then I copied the header, made a new one and changed coordinates keywords. Finally, I put the rotated data with the new header and saved as a new FITS file.

Fortunately, the script worked on the data from CASA tutorials. There is some uncertainty from the observation and process of getting the true data, but for this purpose it is sufficient.

References

- ALMA Czech node (2017), ‘Alma starts observing the sun’. [Online; accessed May 31, 2020].
URL: <https://www.almaobservatory.org/en/announcement/alma-starts-observing-the-sun/>
- ALMA Partnership (2015), ‘The 2014 ALMA Long Baseline Campaign: An Overview’, *The Astrophysical Journal Letters* **808**(1), L1.
- ALMA Science archive (2020), ‘Alma science archive’. [Online; accessed May 31, 2020].
URL: <https://almascience.eso.org/asax/>
- Altschuler, D. R. & Salter, C. J. (2013), ‘The Arecibo Observatory: Fifty astronomical years’, *Physics Today* **66**(11), 43.
- ASTRON (2018), ‘Locations of the lofar telescopes’. [Online; accessed May 31, 2020].
URL: http://old.astron.nl/sites/astron.nl/files/cms/LOFAR_Map_2018.jpg
- Bastian, T. S., Bárta, M., Brajša, R., Chen, B., Pontieu, B. D., Gary, D. E., Fleishman, G. D., Hales, A. S., Iwai, K., Hudson, H., Kim, S., Kobelski, A., Loukitcheva, M., Shimojo, M., Skokić, I., Wedemeyer, S., White, S. M. & Yan, Y. (2018), ‘Exploring the Sun with ALMA’, *The Messenger* **171**, 25–30.
- Born, M. & Wolf, E. (1965), *Principles of optics. Electromagnetic theory of propagation, interference and diffraction of light*.
- Bárta, M. (2016), ‘Sluneční radioastronomie v éře alma’. [Online; accessed May 31, 2020].
URL: <https://www.suh.sk/obs/slnsem/22css/33w.pdf>
- CASA Guide (2018), ‘Sunspot band6 calibration for casa 5.1’. [Online; accessed May 31, 2020].
URL: https://casaguides.nrao.edu/?title=Sunspot_Band6_Calibration_for_CASA_5.1
- Clark, B. G. (1980), ‘An efficient implementation of the algorithm ‘CLEAN’’, *Astronomy and Astrophysics* **89**(3), 377.
- ESO/C., Furtak (2017), ‘The event horizon telescope and global mm-vlbi array on the earth’. [Online; accessed May 31, 2020].
URL: <https://www.eso.org/public/czechrepublic/images/ann17015a/>
- ESO/C., Malin (2012), ‘The atacama large millimeter/submillimeter array (alma) by night, under the magellanic clouds’. [Online; accessed May 31, 2020].
URL: <https://www.eso.org/public/czechrepublic/images/ann12092a/>

Heinzel, P., Berlicki, A., Bárta, M., Karlický, M. & Rudawy, P. (2015), ‘On the Visibility of Prominence Fine Structures at Radio Millimeter Wavelengths’, **290**(7), 1981–2000.

Hey, J. S. (1946), ‘Solar Radiations in the 4-6 Metre Radio Wave-Length Band’, *Nature* **157**(3976), 47–48.

Högbom, J. A. (1974), ‘Aperture Synthesis with a Non-Regular Distribution of Interferometer Baselines’, *Astronomy and Astrophysics Supplement* **15**, 417.

Jansky, K. G. (1933), ‘Radio waves from outside the solar system’, *Nature* **132**(66).

Mario Roberto Durán Ortiz (2019), ‘View of the arecibo radio telescope primary dish and the spherical reflector, arecibo observatory, puerto rico.’. [Online; accessed May 31, 2020].

URL: https://upload.wikimedia.org/wikipedia/commons/7/71/Arecibo_Radiotelescopio_SJU_06_2019-7

Reber, G. (1940), ‘Cosmic static’, *Astrophysical Journal* **91**, 621–624.

Ryle, M., Smith, F. G. & Elsmore, B. (1950), ‘A preliminary survey of the radio stars in the Northern Hemisphere’, *MNRAS* **110**, 508.

Ryle, M. & Vonberg, D. D. (1946), ‘Solar Radiation on 175 Mc./s.’, *Nature* **158**(4010), 339–340.

Schwarz, U. J. (1978), ‘Mathematical-statistical Description of the Iterative Beam Removing Technique (Method CLEAN)’, *Astronomy and Astrophysics* **65**, 345.

Sergey Trukhin (2015), ‘Siberian solar radio telescope’. [Online; accessed May 31, 2020].

URL: <http://wikimapia.org/2093308/Siberian-Solar-Radio-Telescope-SSRT/photo/4951973>

Skokić, I. & Brajša, R. (2019), ‘ALMA Solar Ephemeris Generator’, *arXiv e-prints* p. arXiv:1904.08263.

Task tclean description (2020). [Online; accessed May 31, 2020].

URL: https://casa.nrao.edu/casadocs/casa-5.6.0/global-task-list/task_tclean/about

van Cittert, P. H. (1934), ‘Die Wahrscheinliche Schwingungsverteilung in Einer von Einer Lichtquelle Direkt Oder Mittels Einer Linse Beleuchteten Ebene’, *Physica* **1**(1), 201–210.

White, S. M., Iwai, K., Phillips, N. M., Hills, R. E., Hirota, A., Yagoubov, P., Siringo, G., Shimojo, M., Bastian, T. S., Hales, A. S., Sawada, T., Asayama, S., Sugimoto, M., Marson, R. G., Kawasaki, W., Muller, E., Nakazato, T., Sugimoto, K., Brajša, R., Skokić, I., Bárta, M., Kim, S., Remijan, A. J., de Gregorio, I., Corder, S. A., Hudson, H. S., Loukitcheva, M., Chen, B., De Pontieu, B., Fleishmann, G. D., Gary, D. E., Kobelski, A., Wedemeyer, S. & Yan, Y. (2017), ‘Observing the Sun with the Atacama Large Millimeter/submillimeter Array (ALMA): Fast-Scan Single-Dish Mapping’, **292**(7), 88.

Wilner (2010), ‘Imaging and deconvolution’. [Online; accessed May 31, 2020].

URL: http://www.aoc.nrao.edu/events/synthesis/2010/lectures/wilner_synthesis10.pdf

Wilson, T. L., Rohlfs, K. & Hüttemeister, S. (2009), *Tools of Radioastronomy*, 3 edn, Springer.

Zernike, F. (1938), ‘The concept of degree of coherence and its application to optical problems’, *Physica* **5**(8), 785–795.

Appendix

Script for conversion from Ra/Dec coordinates to HPC coordinates

```
1 # The computer must have installed python 3.5 or newer, it is due to the
2 # new releases from Astropy and Sunpy required it.
3
4 # for running type to terminal:
5 # python3 ALMAtoHPC.py '(here the name of the FITS file)'
```

```
6
7 import matplotlib.pyplot as plt
8 import sys
9 import datetime
10 from datetime import datetime, timedelta
11 from math import radians
12 #===== Importing Numpy, and rotate from Scipy =====#
13 import numpy as np
14 import scipy.ndimage
15 #===== Importing Astropy libraries =====#
16 from astropy.coordinates import SkyCoord, AltAz, EarthLocation
17 import astropy.coordinates
18 import astropy.time as Time
19 import astropy.units as u
20 from astropy.io import fits
21 #===== Importing SunPy libraries =====#
22 import sunpy
23 from sunpy.coordinates import frames, get_sunearth_distance
24 import sunpy.map as smap
25 from sunpy.coordinates.ephemeris import get_sun_P
26
27 #===== Rotation of the data =====#
28
29 def RotationOfMap(im, hdr, obstime):
30
31     print('Rotating map...')
```

```
32
33     hdr_n = hdr.copy() # Copy of header
34     hdr_n['cdelt1'] = abs(hdr['cdelt1'])*3600
35     hdr_n['cdelt2'] = abs(hdr['cdelt2'])*3600
36     hdr_n['ctype1'] = 'HPLN-TAN'
37     hdr_n['ctype2'] = 'HPLT-TAN'
38     hdr_n['cunit1'] = 'arcsec'
39     hdr_n['cunit2'] = 'arcsec'
40
41     del(hdr_n['comment'])
42
43     sun_eph_P = sunpy.coordinates.get_sun_P(obstime) # Solar angle P
44     rota = scipy.ndimage.rotate(im, angle = sun_eph_P.degree ,order=4,
45                                prefilter=False, reshape=False, cval=np.nan) # Rotating the data
```

```
45     return rota, hdr_n
46
47 #===== Getting data and header from the Fits file =====#
48
49 def loadFits(file_):
50
51     print('Loading FITS file...')
52
53     hdu = fits.open(file_) # Loading of data
54     hdr = hdu[0].header # Data header
55     im = hdu[0].data[0,0] # Data
56     return hdu, hdr, im
57
58 #===== Ra/Dec to HPC =====#
59
60 def radec2hpc(ra, de, obstime):
61
62     print('Transforming Ra/Dec to HPC coord...')
63
64     c_rd = SkyCoord(ra=ra*u.rad, dec=de*u.rad, frame='icrs', obstime=obstime)
65         # Writing the right way for the coordinates for Astropy
66
67     alma = EarthLocation.of_site('ALMA') # The global position of ALMA
68
69     distance = sunpy.coordinates.get_sunearth_distance(obstime) # Distance
70         of earth to the Sun for the corresponding date of observation
71
72     fa = AltAz(obstime=obstime, location=alma) # Converting RA and Dec
73         coordinates to AZ and Alt coordinates
74
75     temp = c_rd.transform_to(fa)
76
77     sun_altaz = SkyCoord(az=temp.T.az, alt=temp.T.alt, distance=distance,
78         frame=fa) # Writing the right way for the coordinates for Astropy
79
80     sun_hp = sun_altaz.transform_to(frames.Helioprojective) # Converting
81         from AZ and Alt coordinates to Helioprojective coordinates
82
83     return sun_hp.T.Tx.value, sun_hp.T.Ty.value
84
85 file_ = sys.argv[1]
86 hdu, hdr, im = loadFits(file_)
87
88 #= Getting observation time, reference values from ALMA header =#
89 obstime = Time.Time(hdr['DATE-OBS']) # Observing time
90 ra = radians(hdr['crval1'])
91 dec = radians(hdr['crval2'])
92
93 hdr['crval1'], hdr['crval2'] = radec2hpc(ra, dec, obstime) # x,y coordinate
94     in HPC
95
96 rota, hdr_n = RotationOfMap(im, hdr, obstime)
97 sunpy.io.fits.write('HPC'+file_, rota, hdr_n) # Saving data to new FITS
98     file
```

Script for conversion from Ra/Dec coordinates to HPC coordinates and overlay with SDO/AIA or SDO/HMI data

```
1 # The computer must have installed python 3.5 or newer, it is due to the
2 # new releases from Astropy and Sunpy required it.
3
4 import matplotlib.pyplot as plt
5 from skimage import data, io
6 import datetime
7 from datetime import datetime, timedelta
8
9 #===== Importing Numpy, and rotate from Scipy =====#
10 import numpy as np
11 import scipy.ndimage
12
13 #===== Importing Astropy libraries =====#
14 from astropy.coordinates import SkyCoord, EarthLocation, AltAz
15 import astropy.coordinates
16 import astropy.time as Time
17 import astropy.units as u
18 from astropy.io import fits
19
20
21 #===== Importing SunPy libraries =====#
22 from sunpy.coordinates import frames, get_sunearth_distance
23 import sunpy.map as smap
24 from sunpy.coordinates.ephemeris import get_sun_P
25 import sunpy
26 from sunpy.net import Fido, attrs as a
27
28 class ALMAwithSDO:
29
30
31     def __init__(self, file_, wavelength = None, alpha = None, instrument =
32         None):
33 #===== Folder and Alma fits file =====#
34
35         self.file_ = file_
36         self.hdu, self.hdr, self.im = self.loadFits()
37
38         self.wl = wavelength
39         if not wavelength:
40             self.wl = 304
41
42         self.alpha = alpha
43         if not alpha:
44             self.alpha = 0.5
45
46         self.instrument = instrument
47         if not instrument:
48             self.instrument = 'aia'
49
50 #= Getting observation time, reference values from ALMA header =#
51
52         obstime = self.hdr['DATE-OBS'] # Observing time
53         self.obstime = astropy.time.Time(obstime)
54         ra1 = radians(self.hdr['crval1'])
55         dec1 = radians(self.hdr['crval2'])
```

```
56
57
58     self.sun_eph_P = sunpy.coordinates.sun.P(self.obstime) # Solar
        angle P
59     crval1, crval2 = self.radec2hpc(ra1, dec1, self.sun_eph_P)
60     self.hdr['crval1'] = crval1 # x coordinate in HPC
61     self.hdr['crval2'] = crval2 # y coordinate in HPC
62
63     self.plot()
64
65     def RotationOfMap(self):
66
67         print('Rotating map...')
68
69         hdr_n = self.hdr.copy() # Copy of header
70         hdr_n['cdelt1'] = abs(self.hdr['cdelt1'])*3600
71         hdr_n['cdelt2'] = abs(self.hdr['cdelt2'])*3600
72         hdr_n['ctype1'] = 'HPLN-TAN'
73         hdr_n['ctype2'] = 'HPLT-TAN'
74         hdr_n['cunit1'] = 'arcsec'
75         hdr_n['cunit2'] = 'arcsec'
76
77         del(hdr_n['comment'])
78
79         rota = scipy.ndimage.rotate(self.im, angle = self.sun_eph_P.degree ,
            order=4, prefilter=False, reshape=False, cval=np.nan) # Rotating
            the data
80         return smap.Map(rota, hdr_n) # Creating map
81
82 #===== Getting data and header from the Fits file =====#
83
84     def loadFits(self):
85
86         print('Loading FITS file...')
87
88         hdu = fits.open(self.file_) # Loading of data
89         hdr = hdu[0].header # Data header
90         im = hdu[0].data[0,0] # Data
91         return hdu, hdr, im
92
93 #===== Sun picute from AIA =====#
94
95     def AIASun(self):
96
97         print('Getting AIA picture...')
98
99         end = self.obstime.datetime + timedelta(seconds = 60) # Time
100        attrs_time = a.Time( self.obstime, end)
101        result = Fido.search(attrs_time, a.Instrument('aia'), a.Wavelength(
            self.wl*u.angstrom)) # Finds image from AIA from the same time
102        downloaded_files = Fido.fetch(result) # Path to AIA image
103        argh = fits.open(downloaded_files[0])
104        argh.verify('fix')
105        Sun = argh[1].data # AIA Sun image
106        Sun_head = argh[1].header # AIA Sun header
107        return smap.Map(Sun, Sun_head) # AIA Sun map
108
109 #===== Sun picute from HMI =====#
110
111     def HMISun(self):
```

```
112
113     print('Getting HMI picture...')
114
115     end = self.obstime.datetime + timedelta(seconds = 60) # Time
116     attrs_time = a.Time( self.obstime, end)
117     result = Fido.search(attrs_time, a.Instrument('hmi')) # Finds image
118         from HMI from the same time
119     downloaded_files = Fido.fetch(result) # Path to AIA image
120     argh = fits.open(downloaded_files[0])
121     argh.verify('fix')
122     Sun = argh[1].data # HMI Sun image
123     Sun_head = argh[1].header # HMI Sun header
124     return smap.Map(Sun, Sun_head) # HMI Sun map
125 #===== Ra/Dec to HPC =====#
126
127     def radec2hpc(self, ra, de, sun_P):
128
129         print('Transforming Ra/Dec to HPC coord...')
130
131         c_rd = SkyCoord(ra=ra*u.rad, dec=de*u.rad, frame='icrs', obstime=self.
132             obstime) # Writing the right way for the coordinates for Astropy
133
134         alma = EarthLocation.of_site('ALMA') # The global position of ALMA
135
136         distance = sunpy.coordinates.sun.earth_distance(self.obstime) #
137             Distance of earth to the Sun for the corresponding date of
138             observation
139
140         fa = AltAz(obstime=self.obstime, location=alma) # Converting RA and
141             Dec coordinates to AZ and Alt coordinates
142
143         temp = c_rd.transform_to(fa)
144
145         sun_altaz = SkyCoord(az=temp.T.az, alt=temp.T.alt, distance=distance
146             , frame=fa) # Writing the right way for the coordinates for
147             Astropy
148
149         sun_hp = sun_altaz.transform_to(frames.Helioprojective) #
150             Converting from AZ and Alt coordinates to Helioprojective
151             coordinates
152
153         return sun_hp.T.Tx.value, sun_hp.T.Ty.value
154
155     def CompositeALMAandAIA(self, sSun, xmap):
156
157         print('Composing map...')
158
159         return sunpy.map.Map(sSun, xmap, composite=True) # Composite of the
160             data and Sun image
161
162     def plot(self):
163
164         print('Plotting...')
165
166         xmap = self.RotationOfMap()
167
168         if self.instrument == 'aia':
169             sSun = self.AIASun()
170         if self.instrument == 'hmi':
```

```
162         ssSun = self.HMISun()
163         sSun = ssSun.rotate(order=3)
164
165         # Cutout
166         top_right = SkyCoord((xmap.top_right_coord.Tx.value) * u.arcsec, (
            xmap.top_right_coord.Ty.value) * u.arcsec, frame=xmap.
            coordinate_frame)
167         bottom_left = SkyCoord((xmap.bottom_left_coord.Tx.value) * u.arcsec
            , (xmap.bottom_left_coord.Ty.value) * u.arcsec, frame=xmap.
            coordinate_frame)
168         swap_submap = sSun.submap(bottom_left, top_right)
169
170         comp_map = self.CompositeALMAandAIA(swap_submap, xmap)
171         comp_map.set_alpha(index=1, alpha=self.alpha)
172
173         # Plot settings
174         fig = plt.figure(figsize=(20, 15))
175
176         ax1 = fig.add_subplot(1, 3, 1)
177         xmap.plot(axes=ax1)
178
179         ax2 = fig.add_subplot(1, 3, 2)
180         comp_map.plot(axes=ax2)
181
182         ax3 = fig.add_subplot(1, 3, 3)
183         swap_submap.plot(axes=ax3)
184
185         plt.savefig('{}_with_{}_A.png'.format(self.file_, sSun.instrument
            , sSun.wavelength.value), dpi=200) # Saving the composite image
```

